NONLINEAR VISCOUS WAVES PRODUCED BY AN IMPULSIVELY MOVING PLATE

by
S. A. Yang and Allen T. Chwang

Sponsored by

The Ocean Engineering Division
The Office of Naval Research
Under Grant N00014-89-J-1581

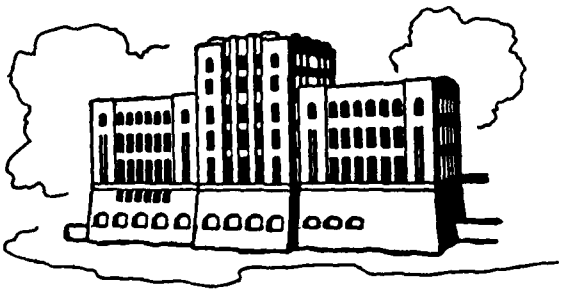

IIHR Report No. 332

Iowa Institute of Hydraulic Research
The University of Iowa
Iowa City, Iowa 52242

September 1989

NONLINEAR VISCOUS WAVES PRODUCED BY AN IMPULSIVELY MOVING PLATE

by

S.A. Yang and Allen T. Chwang

Sponsored by

The Ocean Engineering Division
The Office of Naval Research
Under Grant N00014-89-J-1581

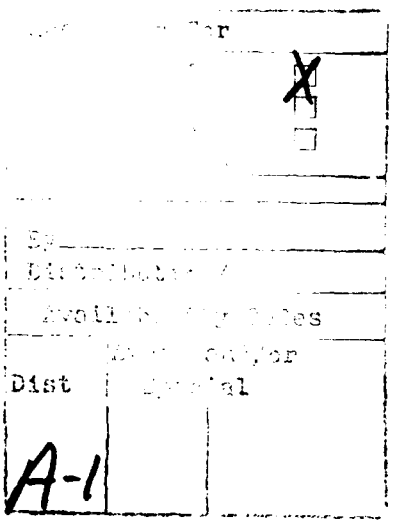

IIHR Report No. 332

Iowa Institute of Hydraulic Research
The University of Iowa
Iowa City, Iowa 52242

September 1989

Unclassified

SECURITY CLASSIFICATION OF THIS PAGE (When Data Entered)

REPORT DOCUMENTATION PAGE		READ INSTRUCTIONS BEFORE COMPLETING FORM
1. REPORT NUMBER IIHR Report No. 332	2. GOVT ACCESSION NO.	3. RECIPIENT'S CATALOG NUMBER
4. TITLE (and Subtitle) Nonlinear Viscous Waves Produced by an Impulsively Moving Plate		5. TYPE OF REPORT & PERIOD COVERED Technical Report 2/1/89 - 9/30/89 6. PERFORMING ORG. REPORT NUMBER IIHR Report No. 332
7. AUTHOR(s) S.A. Yang and Allen T. Chwang		8. CONTRACT OR GRANT NUMBER(s) N00014-89-J-1581
9. PERFORMING ORGANIZATION NAME AND ADDRESS Iowa Institute of Hydraulic Research The University of Iowa Iowa City, Iowa 52242-1585		10. PROGRAM ELEMENT, PROJECT, TASK AREA & WORK UNIT NUMBERS
11. CONTROLLING OFFICE NAME AND ADDRESS The Ocean Engineering Division, The Office of Naval Research, 800 N Quincy Street, Arlington, Virginia 22217-5000		12. REPORT DATE September 1989 13. NUMBER OF PAGES 76
14. MONITORING AGENCY NAME & ADDRESS(if different from Controlling Office) Office of Naval Research Resident Representative, University of Washington, 315 University District Building, 1107 N.E. 45th Street, Seattle, Washington 98105-4631		15. SECURITY CLASS. (of this report) Unclassified 15a. DECLASSIFICATION/DOWNGRADING SCHEDULE
16. DISTRIBUTION STATEMENT (of this Report) Approved for Public Release; Distribution Unlimited		
17. DISTRIBUTION STATEMENT (of the abstract entered in Block 20, if different from Report) Unlimited		
18. SUPPLEMENTARY NOTES		
19. KEY WORDS (Continue on reverse side if necessary and identify by block number) Fluid-Body Interaction, Viscous Waves, Free-Surface Flow, Computational Fluid Dynamics, Experimental Method.		

20. ABSTRACT (Continue on reverse side if necessary and identify by block number)

The free-surface flow generated by an impulsively accelerating, surface-piercing, vertical plate has been studied numerically as well as experimentally. The two-dimensional, unsteady Navier-Stokes equations are discretized using the finite-analytic scheme which incorporates the analytic solution into the locally linearized differential equations. The continuity equation and the dynamic boundary conditions on normal and tangential stresses at the free surface are applied to determine the pressure and two velocity components at the free surface. The kinematic boundary condition on the free surface provides the

DD FORM 1 JAN 73 1473 EDITION OF 1 NOV 65 IS OBSOLETE
S/N 0102-LF-014-6601

Unclassified

SECURITY CLASSIFICATION OF THIS PAGE (When Data Entered)

movement of the free surface.

A series of experiments is carried out in an open channel with a constant water depth. The flat vertical plate is fixed on a towing carriage which is set off by suddenly dropping a weight bucket through a connecting steel cable in a pulley system. A data acquisition system is used for controlling the sampling process and for recording the signal output. The free-surface profile ahead of the plate and the pressure distribution on the plate surface are measured.

The agreement of the free-surface profile and the pressure distribution between the numerical results and the experimental measurements is fairly good. The mathematical singularity, which is predicted by the potential-flow theory, at the contact line between the plate and the free surface is not observed in the physical experiments. The water surface in front of the vertical plate simply rises up during the initial stage of the acceleration of the plate.

TABLE OF CONTENTS

ABSTRACT

The free-surface flow generated by an impulsively accelerating, surface-piercing, vertical plate has been studied numerically as well as experimentally. The two-dimensional, unsteady Navier-Stokes equations are discretized using the finite-analytic scheme which incorporates the analytic solution into the locally linearized differential equations. The continuity equation and the dynamic boundary conditions on normal and tangential stresses at the free surface are applied to determine the pressure and two velocity components at the free surface. The kinematic boundary condition on the free surface provides the movement of the free surface.

A series of experiments is carried out in an open channel with a constant water depth. The flat vertical plate is fixed on a towing carriage which is set off by suddenly dropping a weight bucket through a connecting steel cable in a pulley system. A data acquisition system is used for controlling the sampling process and for recording the signal output. The free-surface profile ahead of the plate and the pressure distribution on the plate surface are measured.

The agreement of the free-surface profile and the pressure distribution between the numerical results and the experimental measurements is fairly good. The mathematical singularity, which is predicted by the potential-flow theory, at the contact line between the plate and the free surface is not observed in the physical experiments. The water surface in front of the vertical plate simply rises up during the initial stage of the acceleration of the plate.

ACKNOWLEDGEMENTS

This research was sponsored by the Ocean Engineering Division, the Office of Naval Research, under Grant N00014-89-J-1581. The assistance provided by IIHR's mechanical and electronics shops is very much appreciated. The authors are grateful to the Graduate College of the University of Iowa and the University of Illinois at Urbana-Champaign for providing the computer funds.

LIST OF SYMBOLS

Alphabetical Symbols

A,B	coefficients in the linearized convective-transport equation (III.1)
A_m	coefficient in equation (V.2)
$a(t)$	plate acceleration
a_1	leading term of a(t)
a_n,a_s,a_w,a_e,a_p	coefficients in equation (III.19)
$\bar{c}_n,\bar{c}_s,\bar{c}_w,\bar{c}_e,\bar{c}_p$	coefficients in equations (III.10) and (III.11)
c_n,c_s,c_w,c_e,c_t,c_p	coefficients in equations (III.13)
d_n,d_s,d_w,d_e	coefficients in equations (III.14) to (III.17)
$\hat{D}$	source term in equation (III.19)
D^*	source term in equation (III.32)
$F(x,y,t)$	free surface equation
Fr	Froude number
f	velocity component u or v
f_n,f_s,f_w,f_e,f_p	velocity component u or v at the nodal grid in the numerical grid system
G_f	nonhomogeneous term in equation (III.3)
g	gravitational acceleration
H	coefficient in equation (III.13)
h_o	unperturbed free-surface level
$h(x,t)$	free-surface elevation
K	surface curvature
k_m	coefficient in equations (V.1) and (V.2)
n_i	x_i component of the unit vector normal to the free surface
p	pressure field

p_n, p_s, p_w, p_e, p_p	pressure at the nodal point
Re	Reynolds number
s_f	source term in equation (III.1)
t	time coordinate
t_i	x_i component of the unit vector tangential to the free surface
U,V	mean values of u and v in the numerical element
u,v	velocity components in the x and y directions respectively
$\hat{u},\hat{v}$	pseudo-velocity components
u^*, v^*	pre-converged velocity components
u', v'	velocity corrections
We	Weber number
x,y	Cartesian coordinates

Greek Symbols

α	acceleration intensity in equation (V.2)
ε	nondimensional time parameter defined in equation (V.3)
δ_{ij}	Kronecker delta
λ_m	coefficient in equation (V.2)
υ	kinematic viscosity of fluid
π	= 3.14159
ρ	density of fluid
σ	coefficient of surface tension
σ_{ij}	stress tensor

LIST OF FIGURES

I. INTRODUCTION

The study of the fluid-body interaction with a free surface has received a considerable interest in the past few decades. The applications extend to a variety of topics, such as designs of dams, bridge piers, offshore structures, ships, and so on. For instance, the information of pressure and velocity distributions around a ship is required in designing a high-performance ship hull. Up to date, the associated design involving the free surface still depends heavily on the towing-tank experiments. However, the exact dynamic similitude in free-surface flows is rarely achieved. It is common to require only Froude number similarity when two systems are compared experimentally. Then the Reynolds number for the model test may be several hundred times less than that for the prototype so that the viscous effects are not properly modelled. Corrections for viscous effects can be made by using models of different scale ratios and extrapolating the results to full prototype scale. Since exact dynamic similitude is rarely achieved in models of free-surface systems, a considerable amount of judgment is necessary both in designing models and in interpreting the results. Alternatively, the numerical experiment may resolve the problem of dynamic similitude which plagues the towing-tank experiment. Once the validity of a computer code is verified, the flow fields subjected to different conditions can be obtained by changing the associated parameters, such as the Reynolds number, the Froude number, and the Weber number, etc. However, the numerical method itself also carries difficulties. The main difficulty arises from determining the time-dependent free-surface profile, which is not only a boundary of the flow field, but also a part of the solution. Furthermore, the researchers are puzzled by the irregular free-surface cells, which make the calculations difficult, when a time-independent Eulerian coordinate system is used. As for the analytical method, Chwang (1983) developed a nonlinear potential-flow theory by using a small-time-expansions method to determine the hydrodynamic pressure on an accelerating vertical plate and the free-surface profile in front of it. A similar problem was studied by Roberts (1987). Wang (1985) extended Chwang's idea to investigate the three-dimensional nonlinear free-surface flow around an impulsively accelerating, surface-piercing, vertical cylinder. A mathematical singularity was predicted at the intersection of the body and the

adjacent free surface by the potential-flow theory. However, the physical singularity was not observed in Wang's experimental study.

I.1 Review of Numerical Study

The free-surface problem was first solved numerically by Welch et al. (1965). The so-called Marker-And-Cell (MAC) method is a technique for solving the time-dependent flow field of a viscous, incompressible fluid with a free surface. This method employed an Eulerian mesh of calculation cells and finite-difference expression to approximate the continuity and Navier-Stokes equations. The marker particles on the free surface were used to identify the free-surface location by applying the kinematic boundary condition. In order to facilitate calculations, the cells in the computational domain were flagged to be body boundary cells, free-surface boundary cells, full cells, or empty cells. The dynamic boundary conditions on the free surface, which required that the normal and tangential stresses be continuous, were used to determine the pressure and velocities on the free surface. However, the MAC method in its original form used simple approximations for these conditions. The normal-stress condition was replaced by zero surface pressure. The tangential-stress condition was replaced by two conditions: one on the fluid incompressibility for surface cells, and another on the vanishing normal derivative of the fluid velocity at the free surface.

Improvements on the MAC method have been achieved later by several researchers. Hirt and Shannon (1968) studied the formation of a viscous bore and recovered the normal-stress boundary condition at the center of the free-surface cells where pressure was calculated. Chan and Street (1970a, 1970b) applied the same boundary condition at the exact free-surface location to determine the run-up of a solitary wave on a vertical wall. In addition to the normal-stress boundary condition, Nicols and Hirt (1971) applied the tangential-stress condition to calculate the free-surface velocity. They simplified the equation by categorizing the free-surface slopes to have only vertical, horizontal, or 45^{o} directions, and investigated a collapsing fluid column, a splashing drop in a deep pool, and a viscous bore. The related studies and improvements were also made by

Hirt, Cook, and Butler (1970), Viecelli (1971), Faltinsen (1977), and Lin, Newman, and Yue (1984). Tang (1987) specified the complete boundary conditions on the free surface using the finite-analytic scheme developed by Chen and his associates (1980-1986). The kinematic boundary condition was used to provide the movement of the free surface. Two dynamic boundary conditions at the free surface were used to determine the pressure and horizontal velocity component respectively. The vertical velocity component was obtained by extrapolation from the flow domain. This is a good approximation for smooth and slowly-varying flow fields only. A refinement can be made by requiring conservation of mass in the surface cell.

Three-dimensional versions of the MAC method with inviscid-flow free-surface boundary conditions have been developed for ship wave problems by Suzuki et al. (1981), Masuko et al. (1982), Miyata and Inui (1984), Miyata and Nishimura (1985), and Miyata et al. (1985). Miyata et al. (1987) incorporated a boundary-fitted curvilinear coordinate system, which was deformed to fit the moving free-surface at each time step, into the computational procedure. A sub-grid-scale model was also introduced by Miyata et al. (1987) to simulate the turbulent flow. Their computer code, in its infant stage, still suffered from the problems of accuracy, stability, and efficiency of calculations. For instance, a filter was applied to the free-surface coordinate to remove the unfavorable fluctuation.

The above-mentioned studies were all based on the finite-difference method. The finite-element formulation for free-surface flows was also developed by a number of authors, including Nickell, Tanner and Caswell (1974), Reddy and Tanner (1978), Frederiksen and Watts (1981), Kawahara and Miwa (1984), and Ramaswamy and Kawahara (1987a, 1987b). In this formulation, the unknowns of the differential equations were discretized using a linear interpolation function, similar to the Galerkin method, based on a three-node triangular finite element.

I.2 Review of Experimental Study

The impulsive start of a wavemaker initially at rest in calm water can simulate the initial stage of the motion of a dam under earthquake loading, or the motion of a ship under sudden acceleration. Greenhow and Lin (1983) took a series of pictures on the free-surface profile in front

of a flat plate moving from rest with a constant velocity. A jet was observed at the contact line. To simulate the slamming of ships, the high speed entry of a wedge and a cylinder into and exit from calm water were also experimented. Because the pictures were taken through the transparent side wall of a tank, the experiments provided the qualitative results due to the viscous and surface-tension effects on the side wall. No pressure measurements were attempted in this study.

Wang (1985) conducted a series of measurements for the free-surface elevation in front of a vertical circular cylinder and for the pressure acting on the cylinder surface. In his experiments, the acceleration of the cylinder was a step function and the velocity was continuous. The agreement between the theoretically predicted values of the free-surface elevation and the experimentally measured ones was fairly good at a distance of at least one radius away from the cylinder surface. His theory over-predicted the hydrodynamic pressure, since no viscous dissipation was included in the inviscid theory.

I.3 Preview of the Present Report

The purpose of the present study is to investigate, numerically as well as experimentally, the initial stage of the flow field generated by a vertical plate accelerating horizontally into a calm water. The unsteady, two-dimensional Navier-Stokes equations are transformed into the corresponding finite-difference form using the finite-analytic scheme developed by Chen and his associates (1980-1986). In this method, the local analytical solutions are obtained for the linearized governing equations in the discretized computational element. The local analytical solutions are then expressed in the algebraic form and are overlapped to cover the entire flow domain. Because of the analytic nature of the solution for the well-posed problem, the numerical solution is more stable and accurate than the conventional finite-difference method. The SIMPLER (Semi-Implicit Method for Pressure-Linked Equations Revised) algorithm of Patankar (1980,1981) is used to solve the discretized equations. The mathematical formulation of the present problem is given in Chapter II and the details of the numerical method are presented in Chapter III.

A series of experiments is conducted in a water flume on the second floor of IIHR. The free-surface profile in front of the plate and pressure distribution on the plate surface are measured for three different accelerations of the plate. A capacitance-type wave gauge is used to measure the variations of the water surface. A variable reluctance pressure transducer is used to measure the surface pressure. An accelerometer is used to measure the acceleration of the plate. All response voltage outputs are recorded on an IBM PC-XT personal computer with a data acquisition electrical board. The setup and experimental procedures are included in Chapter IV.

The experiments are carefully conducted and used as a criterion for evaluating Chwang's theory (1983) and the present numerical code. The comparison and discussion are included in Chapter V.

Finally, conclusions and further extension of present work are presented in Chapter VI.

II. MATHEMATICAL FORMULATION

A vertical, rigid plate is initially at rest at x=0 plane in a channel with a constant fluid depth h_o (Figure 1). At time $t=0_+$, it starts to accelerate horizontally towards the fluid with an acceleration a(t). For a two-dimensional flow of a viscous, incompressible fluid, the continuity and momentum equations in a Cartesian coordinate system (x,y) are

$$\frac{\partial u}{\partial x} + \frac{\partial v}{\partial y} = 0 , \tag{II.1}$$

$$\frac{\partial u}{\partial t} + u\frac{\partial u}{\partial x} + v\frac{\partial u}{\partial y} = -\frac{1}{\rho}\frac{\partial p}{\partial x} + \upsilon\left(\frac{\partial^2 u}{\partial x^2} + \frac{\partial^2 u}{\partial y^2}\right) , \tag{II.2}$$

$$\frac{\partial v}{\partial t} + u\frac{\partial v}{\partial x} + v\frac{\partial v}{\partial y} = -\frac{1}{\rho}\frac{\partial p}{\partial y} + \upsilon\left(\frac{\partial^2 v}{\partial x^2} + \frac{\partial^2 v}{\partial y^2}\right) , \tag{II.3}$$

where u and v are velocities in the x and y directions respectively, p the hydrodynamic pressure, ρ the fluid density, and υ the kinematic viscosity of fluid.

We assume that the acceleration a(t) can be expressed as a power series in t,

$$a(t) = \sum_{n=1}^{\infty} n\, a_n\, t^{n-1} , \tag{II.4}$$

where a_1 is not equal to zero for an impulsive motion. A set of dimensionless quantities can be defined in the following manner:

$$x^o = \frac{x}{h_o}, \qquad y^o = \frac{y}{h_o},$$

$$u^o = \frac{u}{\sqrt{a_1\, h_o}}, \qquad v^o = \frac{v}{\sqrt{a_1\, h_o}}, \tag{II.5}$$

$$p^o = \frac{p}{\rho\, a_1\, h_o}, \qquad t^o = t\sqrt{\frac{a_1}{h_o}},$$

where a_1 is the leading term of equation (II.4) and h_o is the unperturbed free-surface level. Then the dimensionless forms of the governing equations can be written as (after dropping the superscripts 'o')

$$\frac{\partial u}{\partial x} + \frac{\partial v}{\partial y} = 0, \tag{II.6}$$

$$\frac{\partial u}{\partial t} + u\frac{\partial u}{\partial x} + v\frac{\partial u}{\partial y} = -\frac{\partial p}{\partial x} + \frac{1}{Re}\left(\frac{\partial^2 u}{\partial x^2} + \frac{\partial^2 u}{\partial y^2}\right), \tag{II.7}$$

$$\frac{\partial v}{\partial t} + u\frac{\partial v}{\partial x} + v\frac{\partial v}{\partial y} = -\frac{\partial p}{\partial y} + \frac{1}{Re}\left(\frac{\partial^2 v}{\partial x^2} + \frac{\partial^2 v}{\partial y^2}\right), \tag{II.8}$$

where Re denotes the Reynolds number

$$Re = \frac{\sqrt{a_1\, h_o}\, h_o}{\upsilon}.$$

The dependent variables u, v, and p can be solved by the above three equations with specified initial and boundary conditions.

Let F(x,y,t)=0 describe a surface S(t). If S(t) is an interface between two immiscible fluids, the first condition it must satisfy is a kinematic one. As the surface moves, there should be no transfer of matter across the surface. Consequently, the following equation must be satisfied

$$\frac{DF}{Dt} = 0. \tag{II.9}$$

This condition is satisfied by any bounding surface, whether a free surface or a rigid boundary. If the free-surface profile is defined by

$$F(x,y,t) = y - h(x,t) , \tag{II.10}$$

where h(x,t) denotes the free-surface elevation, then the kinematic boundary condition becomes

$$\frac{\partial h}{\partial t} + u \frac{\partial h}{\partial x} = v . \tag{II.11}$$

This condition provides the movement of the free surface.

In addition to the kinematic condition, there are dynamic conditions to be satisfied at the free surface as follows:

1. The effect of surface tension, as one passes through the free surface, is to produce a discontinuity in the normal stress proportional to the mean curvature of the free surface.
2. For a viscous fluid, the tangential stress must be continuous as one passes through the free surface.

The mathematical expressions of the above statements can be written as

$$n_i \sigma_{ij} n_j = \frac{K}{We} , \qquad We = \frac{\rho a_1 h_o^2}{\sigma} , \tag{II.12}$$

and

$$t_i \sigma_{ij} n_j = 0 \qquad (i=1,2;\ j=1,2) , \tag{II.13}$$

where n_i (t_i) is the i-component of a unit vector normal (tangential) to the free surface, σ_{ij} the stress tensor, K the surface curvature, We the Weber number, and σ the surface tension coefficient. The repeated index is summed from 1 to 2. The stress tensor σ_{ij} for an incompressible Newtonian fluid can be expressed as

$$\sigma_{ij} = - (p - \frac{y-1}{Fr^2}) \delta_{ij} + \frac{1}{Re} (\frac{\partial u_j}{\partial x_i} + \frac{\partial u_i}{\partial x_j}) , \tag{II.14}$$

$$Fr^2 = \frac{a_1}{g},$$

where Fr denotes the Froude number, g the gravitational constant, and δ_{ij} the Kronecker delta.

Substituting equation (II.14) into equations (II.12) and (II.13), we have

$$-\left(p - \frac{y-1}{Fr^2}\right) + \frac{2}{Re}\left(\frac{\partial u}{\partial x} n_1^2 + \frac{\partial v}{\partial y} n_2^2\right) + \frac{2}{Re}\left(\frac{\partial u}{\partial y} + \frac{\partial v}{\partial x}\right) n_1 \; n_2 = \frac{K}{We}, \tag{II.15}$$

$$\frac{2}{Re}\left(\frac{\partial u}{\partial x} - \frac{\partial v}{\partial y}\right) n_1 \; n_2 + \frac{1}{Re}\left(\frac{\partial u}{\partial y} + \frac{\partial v}{\partial x}\right)\left(n_2^2 - n_1^2\right) = 0. \tag{II.16}$$

The x and y components of the unit outward normal vector to the free surface are

$$n_1 = -\frac{\partial \eta}{\partial x}\left(1 + \left(\frac{\partial \eta}{\partial x}\right)^2\right)^{-1/2}, \tag{II.17}$$

$$n_2 = \left(1 + \left(\frac{\partial \eta}{\partial x}\right)^2\right)^{-1/2}, \tag{II.18}$$

where η denotes the free-surface variation from the unperturbed water surface. The free-surface curvature is

$$K = \frac{\partial^2 \eta}{\partial x^2}\left(1 + \left(\frac{\partial \eta}{\partial x}\right)^2\right)^{-3/2}. \tag{II.19}$$

The sign is so selected that the normal component of the stress vector increases in the outward normal direction.

Equations (II.15) and (II.16) are used to determine the pressure and horizontal velocity component respectively at the free surface. The vertical velocity component is obtained by applying the continuity equation at the free surface. The no-slip boundary condition is applied at the solid surface except the contact line between the plate and the free surface. The boundary condition in the region around the contact line is still unknown. Several slip boundary conditions similar to the linear slip-shear relation (Lamb, 1932, p.586) were proposed to study the contact-line problem (for example, Hocking (1976), Dussan (1976), Durbin (1988)). None of them are verified theoretically or experimentally. In the numerical calculations, Miyata et al. (1987) applied the no-slip boundary condition at the contact line and calculated the wave height on the body surface by extrapolation from two outer values. In Tang's study (1987), the no-slip boundary condition was released at two nodal points beneath the free surface. The slip velocities were extrapolated from the flow domain. Tang's model seems more reasonable and is adopted in the present study. The initial condition are simply zero velocity and pressure at t=0.

III. NUMERICAL FORMULATION

III.1 Discretization of Governing Equations

In order to solve the velocity and pressure fields numerically, the governing differential equations have to be transformed into the corresponding discretized forms. All variables are assumed to exist at the nodal points only and related to those at the neighboring nodal points by some coefficients obtained from the discretization method. Mathematically, the discretized equations should recover the differential equations if an infinite number of grid points, an infinite small time step, and an appropriate discretization method are used. In other words, the accuracy of the numerical solution depends on the grid size, the increment of the time step, the discretization method, the calculational method, and so on. The finite-analytic scheme, a branch of the finite-difference method, of Chen and others (1980-1986) is used in this study.

The governing equations (II.7) and (II.8) are rewritten in the form

$$\frac{\partial^2 f}{\partial x^2}+\frac{\partial^2 f}{\partial y^2}=2A\frac{\partial f}{\partial x}+2B\frac{\partial f}{\partial y}+Re\frac{\partial f}{\partial t}+S_f, \qquad \text{(III.1)}$$

where f stands for the velocity component u or v, and

$$A=\frac{Re\,U}{2}, \qquad B=\frac{Re\,V}{2},$$

$$S_u=Re\frac{\partial p}{\partial x}, \qquad S_v=Re\frac{\partial p}{\partial y}. \qquad \text{(III.2)}$$

The nonlinear equations have been linearized by replacing the coefficients u and v by U and V respectively in the convective terms, where U and V are mean values of u and v in an numerical element. This approximation is valid for a slowly-varying flow field or for a relatively small element. In the original version of the finite-analytic scheme, the value of a dependent variable at a nodal point was related to those at all neighboring nodal points. This eight-point formula, in a two-dimensional system, ended up with a calculation involving an infinite series for obtaining the

finite-analytic coefficients. Because the method possesses a built-in, automatic upwind nature, the coefficients have to be evaluated at each iteration according to the newly calculated flow field. Therefore, a considerable amount of CPU time makes the method not efficient. Without losing the nature of the original method, a simplified four-point version was derived by Chen and Patel (1987). They tested a uniform flow past a horizontal plate with finite length and obtained fairly good results. Later, Tang (1987) and Richmond (1987) incorporated this simplified version into their studies. We also adopt this four-point finite-analytic method to discretize the governing equations.

The finite-analytic coefficients for nonuniform grids shown in Fig.2(a) are obtained by an exponential-linear scheme. Equation (III.1) is written as

$$\frac{\partial^2 f}{\partial y^2} = 2B \frac{\partial f}{\partial y} + G_f \,, \tag{III.3}$$

where G_f is the nonhomogeneous term

$$G_f = 2A \frac{\partial f}{\partial x} - \frac{\partial^2 f}{\partial x^2} + Re \frac{\partial f}{\partial t} + S_f \,. \tag{III.4}$$

When the boundary conditions along the y-direction are expressed as a linear combination of exponential and linear functions in terms of the nodal values, equation (III.3) can be solved analytically in every numerical element. Let

$$f = a \left(e^{2By} - 1 \right) + b\, y + c \,. \tag{III.5}$$

At the nodal points,

$$y = 0 \quad , \quad f_p = c \,,$$

$$y = h_n \ , \quad f_n = a\,(e^{2Bh_n} - 1) + b\,h_n + c \ ,$$

$$y = -h_s \ , \quad f_s = a\,(e^{-2Bh_s} - 1) - b\,h_s + c \ ,$$

where a, b, and c are solved in terms of the variables f_p, f_n, and f_s as

$$a = \frac{h_n\, f_s + h_s\, f_n - f_p\,(h_n + h_s)}{h_n\, e^{-2Bh_s} + h_s\, e^{2Bh_n} - h_n - h_s} \ , \tag{III.6}$$

$$b = \frac{f_s\,(-e^{2Bh_n} + 1) + f_n\,(e^{-2Bh_s} - 1) + f_p\,(-e^{-2Bh_s} + e^{2Bh_n})}{h_n\, e^{-2Bh_s} + h_s\, e^{2Bh_n} - h_n - h_s} \ , \tag{III.7}$$

$$c = f_p \ . \tag{III.8}$$

At y = 0, equation (III.3) becomes

$$0 = 2Bb + G_f \ . \tag{III.9}$$

Substituting (III.7) into (III.9) and rearranging the terms, we obtain

$$f_p = \tilde{c}_s\, f_s + \tilde{c}_n\, f_n + \tilde{c}_p\, G_f \ , \tag{III.10}$$

where

$$\tilde{c}_s = \frac{e^{2Bh_n} - 1}{e^{2Bh_n} - e^{-2Bh_s}} \ ,$$

$$\bar{c}_n = \frac{1 - e^{-2Bh_s}}{e^{2Bh_n} - e^{-2Bh_s}} ,$$

$$\bar{c}_p = \frac{1}{2B} \frac{-h_s e^{2Bh_n} - h_n e^{-2Bh_s} + h_n + h_s}{e^{2Bh_n} - e^{-2Bh_s}} .$$

We may approximate the x-derivative using the same method as above and obtain

$$2A \frac{\partial f}{\partial x} - \frac{\partial^2 f}{\partial x^2} = - (\bar{c}_w + \bar{c}_e) f_p + \bar{c}_w f_w + \bar{c}_e f_e , \qquad \text{(III.11)}$$

where

$$\bar{c}_w = 2A \frac{1 - e^{2Ah_e}}{h_e e^{-2Ah_w} + h_w e^{2Ah_e} - h_w - h_e} ,$$

$$\bar{c}_e = 2A \frac{e^{-2Ah_w} - 1}{h_e e^{-2Ah_w} + h_w e^{2Ah_e} - h_w - h_e} .$$

The time derivative is approximated by an implicit, backward difference scheme

$$\frac{\partial f_p^n}{\partial t} = \frac{1}{\Delta t} (f_p^n - f_p^{n-1}) , \qquad \text{(III.12)}$$

where f_p^n is the value of f_p at the nth time step, Δt is the increment of the time step. From equations (III.10) to (III.12), we obtain the discretized equation (the superscript n is omitted hereafter for simplicity)

$$f_p = c_s f_s + c_n f_n + c_w f_w + c_e f_e + c_t f_p^{n-1} + c_p S_f , \qquad \text{(III.13)}$$

where

$$c_s = \bar{c}_s H , \qquad c_n = \bar{c}_n H ,$$

$$c_w = \bar{c}_w \bar{c}_p H , \qquad c_e = \bar{c}_e \bar{c}_p H ,$$

$$c_t = - \frac{\bar{c}_p Re}{\Delta t} H , \qquad c_p = \bar{c}_p H ,$$

$$H = \frac{1}{1 + \bar{c}_p (\bar{c}_w + \bar{c}_e - \frac{Re}{\Delta t})} .$$

The variable f_p is now related to those at four neighboring nodes, f_p at the previous time step, and the pressure gradient. With given initial and boundary conditions, the velocity field is calculated from equation (III.13). The pressure field is obtained indirectly via the continuity equation. The numerical method is given in the next section.

III.2 Numerical Method of Solution

The SIMPLER algorithm of Patankar (1981) is adopted to solve the velocity and pressure fields in the flow domain. The arrangement of velocities and pressure at nodal points in a staggered grid system, first proposed by Welch (1965), is shown in Figure 2(b). Because the pressure is obtained via the continuity equation, we separate the pressure terms from other terms in the discretized momentum equation (III.13)

$$u_e = \hat{u}_e + d_e (p_e - p_p) , \qquad \text{(III.14a)}$$

where $\hat{u}_e$, called the pseudo-velocity by Patankar, is defined as

$$\hat{u}_e = \sum_{i=1}^{4} c_{ie} u_{ie} + c_t u_e^{n-1} \qquad \text{(III.14b)}$$

and $$d_e = \frac{Re\, c_p}{\Delta x_e},$$

where the subscript 'ie' denotes the neighboring nodes of node e. Similarly, we can write

$$u_w = \hat{u}_w + d_w (p_p - p_w), \tag{III.15}$$

$$v_n = \hat{v}_n + d_n (p_n - p_p), \tag{III.16}$$

$$v_s = \hat{v}_s + d_s (p_p - p_s). \tag{III.17}$$

Substituting equations (III.14) to (III.17) to the discretized continuity equation

$$(u_e - u_w)\,\Delta y + (v_n - v_s)\,\Delta x = 0, \tag{III.18}$$

we have

$$a_p p_p = a_e p_e + a_w p_w + a_n p_n + a_s p_s + \hat{D}, \tag{III.19}$$

where the coefficients are defined as

$$a_e = \Delta y\, d_e, \quad a_w = \Delta y\, d_w,$$

$$a_n = \Delta x\, d_n, \quad a_s = \Delta x\, d_s,$$

$$a_p = a_e + a_w + a_n + a_s,$$

$$\hat{D} = (\hat{u}_e - \hat{u}_w)\,\Delta y + (\hat{u}_n - \hat{u}_s)\,\Delta x.$$

In this fashion, the pressure field can be obtained from a given velocity field which is contained in the source term $\hat{D}$.

The velocity field is solved from the momentum equation based on a given pressure field. However, the pressure field is obtained via equation (III.19) by a given velocity field. Therefore, an iterative method is necessary to find the final solution based on an initially guessed pressure field. Before a specified convergence criterion is reached, the pre-converged velocity field based on a pre-converged pressure field p^* is denoted by u^* and v^*. The pre-converged velocities can be expressed as

$$u_e^* = \hat{u}_e^* + d_e (p_p^* - p_w^*) . \qquad \text{(III.20)}$$

$$u_w^* = \hat{u}_w^* + d_w (p_p^* - p_w^*) , \qquad \text{(III.21)}$$

$$v_n^* = \hat{v}_n^* + d_n (p_n^* - p_p^*) , \qquad \text{(III.22)}$$

$$v_s^* = \hat{v}_s^* + d_s (p_p^* - p_s^*) . \qquad \text{(III.23)}$$

Equations (III.20) to (III.23) for the velocity field and equation (III.19) for the pressure field provide a complete discretized system for the numerical calculation.

In order to accelerate the speed of convergence, the resulting velocity field at each iteration can be corrected by requiring that the velocity field satisfy the continuity equation. Let us define the velocity corrections u', v' and the pressure correction p' as

$$u' = u - u^* , \quad v' = v - v^* , \quad p' = p - p^* ,$$

where u, v, p are converged values, and u^*, v^*, p^* are pre-converged values. From equations (III.14) and (III.20), we have

$$u_e' = \hat{u}_e' + d_e (p_e' - p_p') , \tag{III.24}$$

where $\hat{u}_e' = \hat{u}_e - \hat{u}_e^*$. Similarly,

$$u_w' = \hat{u}_w' + d_w (p_p' - p_w') , \tag{III.25}$$

$$v_n' = \hat{u}_n' + d_n (p_n' - p_p') , \tag{III.26}$$

$$v_s' = \hat{v}_s' + d_s (p_p' - p_s') . \tag{III.27}$$

For convenience, we may drop $\hat{u}_e'$, $\hat{u}_w'$, $\hat{v}_n'$, and $\hat{v}_s'$. Then, the velocity-correction formula can be written as

$$u_e = u_e^* + d_e (p_e' - p_p') , \tag{III.28}$$

$$u_w = u_w^* + d_w (p_p' - p_w') , \tag{III.29}$$

$$v_n = v_n^* + d_n (p_n' - p_p') , \tag{III.30}$$

$$v_s = v_s^* + d_s (p_p' - p_s') . \tag{III.31}$$

Substituting equations (III.28) to (III.31) into the discretized continuity equation, we have

$$a_p p'_p = a_n p'_n + a_s p'_s + a_e p'_e + a_w p'_w + D^*, \qquad \text{(III.32)}$$

where

$$D^* = (u^*_e - u^*_w) \Delta y + (v^*_n - v^*_s) \Delta x .$$

The pressure-correction p' is obtained from the pre-converged velocity field which appears in the source term D^*. Note that omitting any terms in the equations may result divergence or lead to wrong solutions. However, the terms we have dropped will approach zero when the solutions converge and will not affect the ultimate solutions in this case. The corrected velocity field satisfies the continuity equation at every iteration cycle. The numerical computation is prone to convergence and a continuity-satisfying velocity field is physically more reasonable than the uncorrected velocities in equations (III.20) to (III.23).

III.3 Solution Procedure

We have derived all the required discretized equations and in a position to describe the sequence of calculational operations. The numerical computation is done according to the following steps:

1. Define the physical domain and generate a suitable numerical grid system.
2. Specify the initial condition.
3. Specify the boundary conditions which are time dependent in the present study.
4. Calculate the finite-analytic coefficients given in (III.13), (III.10), and (III.11).
5. Calculate velocities u^* and v^* from equations (III.20) to (III.23) and obtain D^*.
6. Calculate pressure-correction p' from equation (III.32).
7. Correct the velocity field by means of equations (III.28) to (III.31).
8. Calculate pseudo-velocities $\hat{u}$ and $\hat{v}$ from (III.14b) and obtain $\hat{D}$ from (III.19).
9. Calculate pressure p from equation (III.19).

10. Calculate free-surface velocities and pressure from dynamic boundary equations, (II.15) and (II.16) and continuity equation, (II.6).
11. Repeat steps 4 to 10 until both the velocity and pressure fields reach a specified convergence criterion. In the present study, the absolute error is 10^{-6} or less.
12. Use the kinematic boundary condition (II.11) to update the free-surface elevation and use the given boundary condition to determine the new position of the plate.
13. Return to step 3 for the next time step.
14. Stop if time exceeds the specified maximum time period.

IV. EXPERIMENTAL STUDY

The purpose of the experiments is to measure the free-surface profile and the pressure distribution on an impulsively moving plate subject to various accelerations. The experimental setup and procedures will be presented. The features of each instrument used in the present experiments will be discussed.

IV.1 Experimental Model

A series of experiments was conducted in a water flume on the second floor of Iowa Institute of Hydraulic Research. The 26m-long, 0.8m-wide, 0.3m-high open channel with transparent glass bottom and sides is tiltable through an electrical driven gear system. The zero slope was adjusted from a counter mechanically attached on the gear system. A level was used to double-check manually the channel slope and to make sure no local humps on the channel bottom in the test reach. A towing carriage was constrained to move along a pair of parallel rails mounted on the top of the side walls of the channel (Figure 3). The carriage was set off impulsively by suddenly dropping a weight bucket through a connecting steel cable in a pulley system. A plexiglass flat plate was fixed on the carriage vertically and traversely. The channel was filled with water to a height of 10cm. In order to diminish quickly the water disturbance generated by the previous run between two measurements, the channel was shortened to 6m by putting two wood boards upstream and downstream traversely. There was a moment acting on the moving plate due to the relative motion of water. After a few test runs, we found that the impulsively moving carriage was tilted and even overturned by this moment. We then decided to narrow the width of the channel to 20cm by putting a wood board longitudinally. The carriage, with the narrowed plate, ran smoothly after the modification. Therefore, the final dimension of the experimental channel is 6mx0.2mx0.3m together with a 0.2mx0.3m plexiglass flat plate fixed on an instrument carriage (Figure 3).

IV.2 Instrumentation

IV.2.1 Acceleration Transducer

A Kyowa ASQ-2BL servo-type acceleration transducer (Figure 4) with a $\pm 2*9.81 m/sec^2$ capacity was mounted on the carriage to measure the acceleration. It provides a wide frequency response range and permits faithful measurement of random wave forms because of its excellent phase characteristics. Unlike conventional strain-gauge-based transducers, the ASQ-2BL accelerometer is equipped with a servomechanism to measure very small vibration with high accuracy, which is difficult to measure with conventional transducers. For the conventional transducers, the response voltage output is transmitted through an electrical cable and amplified by a signal conditioner. The signal distortions and noises, produced by the cable and by the signal conditioner, are also amplified inevitably. The outcome makes the data analysis difficult. The longer the cable is, the worse the contamination will be. The Kyowa accelerometer overcomes this difficulty by a built-in amplifier which provides a 5-volt output in the full scale. This feature improves the stability and reliability of the response signals received by the signal conditioner. The Kyowa VAQ-500A signal conditioner is a multi-purpose vibration measuring instrument designed primarily for use with the above-mentioned accelerometer. Combined with the signal conditioner, the accelerometer can not only measure the acceleration, but also the velocity and displacement. Before the operation, a warm-up time of at least 2 hours is required after power is supplied.

The calibration was done following the procedure in the user's manual. Because the accelerometer has a high DC sensitivity, calibration can be done via the gravitational acceleration without using special equipment. The general calibration steps are:

1. Decide the maximum value of acceleration in the experiments.
2. Set the measuring ange. There are five measuring ranges, 1%, 3%, 10%, 30%, and 100% of the full scale, to be chosen.
3. Place the accelerometer horizontally and set the output voltage to 0 V. Because the gravitational acceleration applied in thc vibration detecting direction is 0 G in this condition, the output voltage is zero.

4. Tilt the accelerometer to the position where the maximum acceleration is applied and set the output voltage to 5 V.
5. Repeat steps 3 and 4 several times until both 0 and 5 output voltages do not shift.
6. Tilt the accelerometer to several intermediate positions.
7. Repeat steps 3 to 6 several times. Average the measurements at each position and plot a calibration curve. A typical calibration curve is shown in Figure 5.

The acceleration can be measured in a frequency range from 0 to 370 Hz by the Kyowa accelerometer. Although the user's manual does not suggest a dynamic calibration, the above calibration curve is thought, by experience, to be valid for the frequencies lower than 100Hz. For frequencies higher than 100Hz, the calibration curve has to be examined by dynamic response measurements. A vibrating table with adjustable acceleration and frequency can be used for this purpose. As for our experiments, the acceleration is a step function with a nearly constant value. Therefore, the static calibration curve is applicable to our study.

IV.2.2 Pressure Transducer

A Validyne DP-15 variable reluctance pressure transducer (Figure 6) was used to measure the pressure on the moving plate. This differential transducer is equipped with 2 pressure ports and 2 bleed ports. A wide pressure range from 0.125 to 3200 psi can be measured by replacing a diaphragm of magnetically permeable stainless steel inside the transducer which can be disassembled. A diaphragm of 0.125-psi capacity is used in the present experiments. The transducer with an applied pressure generates an AC signal which is transmitted through an electrical cable to a signal conditioner. The Validyne CD15 signal conditioner takes this AC signal input, amplifies it, demodulates it, and filters it into a DC voltage which represents the pressure polarity and magnitude. A warm-up time of at least 2 hours is required after power is supplied.

Before any calibration, we first connect a flexible plastic tubing to each pressure port and fill the transducer and tubings with water. It is very important that the pressure cavity and transducer connections are free of air bubbles. Otherwise, the entrapped air bubbles act as a

pneumatic spring and can seriously decrease the frequency response of the measuring system. To assure water fill, loosen the bleed screw with the system pressure on. After the internal gas has been expelled, the water starts flowing out of the bleed port. When this happens, close the screw tight. After expelling the air bubbles, we fix one of the tubings and the transducer in a certain position. Another tubing is attached to a scale which can be moved up and down vertically. The scale is equipped with a vernier so that up to the third digit number, 0.001 foot, can be read. The general calibration steps are:

1. Adjust the movable tubing until free surfaces inside two tubings are on the same level. Set the output voltage to 0 V.
2. Raise the movable tubing to the position where the maximum pressure is applied and set the output voltage to 5 V.
3. Repeat steps 1 and 2 until output voltages 0 and 5 V do not shift.
4. Raise the movable tubing to other intermediate positions. Record the output voltages.
5. Repeat steps 1 to 4 several times and average the output voltages at each position. Plot the calibration curve.

A typical calibration curve is shown in Figure 7. Note that all the connecting plastic tubings should be arranged as short as possible so that any unnecessary errors can be avoided.

IV.2.3 Wave-Height System

A new version of the capacitance-type wave-height system (Figure 8) developed by the IIHR Electronics Shop was used in this study. This new system replaces the old one with much needed improvements in the areas of versatility and sensitivity. The probe interface circuit (signal conditioner) is modular in construction to minimize cost and to allow single probe use or easy expansion to multiple probes.

The probe is made up of three basic parts: the sensor wire, the sensor wire support, and the connecting cable to the interface. The probe sensor consists of a single strand 0.01" diameter copper wire with a Teflon insulation thickness of 0.001". The sensor wire support is constructed

of 0.25" diameter stainless steel tubing in a "U" configuration. In the ends of the support there are inserted lucite insulators which seal the ends of the tubing, provide a convenient attachment point for the sensor wire, and electrically insulate the sensor wire from the support. The sensor wire serves as one plate, the Teflon insulation serves as the dielectric, and the water serves as the other plate of the capacitor. As the probe is immersed in water, the plate area of the capacitor is, in effect, increased proportionally and thereby increases capacitance.

The interface amplifies the input voltage and has a selectable bipolar range of 5 or 10 V full scale. It provides a maximum measurement resolution of approximately 0.002" (0.008 cm) and outputs 300 unique measurements per second. It is important to keep the connecting cable as short as possible and use a cable with rated capacitance as low as possible to achieve a maximum measurement sensitivity.

The dielectric insulator slowly absorbs water that causes a change of capacitance, and consequently a drift of output voltage. After the probe has been immersed in water for about 6 hours, the drift rate is diminished considerably, and after 24 hours of immersion the drift rate becomes very slow. Therefore, the probe must be immersed in water at least 1 to 2 days before taking any measurements. During the experimental period, the probe should be immersed in water completely when not in use and raises to its operating height during tests.

The output signal becomes very unstable when the immersed probe is attached with impurities and air bubbles in water. The flume was cleaned and filled with fresh tap water at the beginning of the experiments. Most air bubbles can leave the water after about 2 days. Thereafter, the sensor wire and support were cleaned periodically by a piece of soft linen sopped with ethyl alcohol during the entire period of experiments.

The wave-height system was calibrated as a set in still water immediately before and after each series of runs. Figure 9 shows a typical static calibration curve. Normally, a dynamic calibration is required to examine the meniscus, wetting, and wake effects in the vicinity of the immersed wire. The commonly used instruments for the dynamic examination consist of an oscillator and an electric motor. The oscillator allows vertical and orbital oscillations of the wave

probe abc ·e the water surface. The amplitudes and periods of the oscillation are adjusted to simulate waves which would be typical of those created in the towing tank. The geared electric motor drives a motion linkage through a transmission allowing continuous variable periods. A thorough study on the dynamic calibration of capacitance, resistance, sonic wave probes was done by Pearlman (1963). He found that the maximum error, which was compared with the static calibration curve, was less than 1% for the capacitance wave probe in the condition of a period range from 0.8 to 2.0 seconds and an amplitude range from 2 to 3 inches. The dynamic calibration was not made in the present study for lack of the required instruments. However, an indirect dynamic examination was carried out by Dr. Toda, a Visiting Scholar of IIHR. He conducted a series of experiments, in the towing tank of IIHR, on ship waves. These experiments were the same as those he had done in Japan (unpublished). A dynamic calibration was made in the experiments which were performed in the towing tank in the Department of Naval Architecture, Osaka University. After the comparison, Dr. Toda concluded that the maximum error of the static calibration curve made from IIHR's probe is ±0.5mm in the condition of a 0.5 second maximum period and a 3cm maximum amplitude. In our experiments, the water surface simply piled up with a maximum amplitude approximately 2cm on a moving plate. Therefore, the static calibration curve was used in the present experiments.

IV.3 Data-Acquisition System

The data-acquisition system is a microcomputer IBM PC/XT with a MetraByte DAS-8 8 channel A/D converter board and a MetraByte STA-08 screw terminal connector board. The data-acquisition board takes signals from measuring devices, converts them to digital forms, and transmits them to the computer in a digital format. The Notebook, a data-acquisition software developed by the Laboratories Technology Corp., was used to define the channel number, the sampling rate, the sampling time length, data file name, and so on.

IV.4 System Setup and Experimental Procedures

All relevant instruments have been familiarized and calibrated following the procedures stated in the previous sections. The accelerometer, wave probe, and pressure transducer were fixed on the carriage and transmitted response output signals through cables to the corresponding signal conditioners and microcomputer which were put on a desk beside the flume. Both pressure and free-surface profile measurements were recorded for a time length about 3 seconds with 100 Hz sampling rate after the carriage was set off. Every measurement was repeated several times for reliable experimental results. A typical response voltage output for acceleration, pressure, and free-surface variation is shown in Figure 10. A time interval of about 5 minutes was necessary between two measurements in order to diminish the water disturbance induced by the previous run.

The wave probe mounted system (Figure 11) was so designed that the probe wire was located at the center of the experimental channel and could be moved to any desired position along the longitudinal direction. Moreover, the probe could be moved up and down so that the calibration could be carried out conveniently before and after a series of runs. In the present experimental study, three accelerations were investigated: a_1=1.04-0.96t, a_2= 0.78-0.69t, and a_3=0.50-0.44t m/sec^2. Ten positions were measured from 0.5cm to 23.5cm away from the plate. The calibration curve was made at each measuring point.

The measurements of the pressure were separated from that of the free-surface profile. This is to avoid the disturbance induced by the wave probe on the pressure taps. The pressure distribution on the plate was measured with 6 1mm-diameter pressure taps located at 2.5, 3.5, 5.0, 6.5, 7.5, and 8.5 cm respectively above the channel bottom. A plastic tubing connected the pressure tap to the '+'ve pressure port of the pressure transducer. The pressure transducer was mounted on the carriage in an upward position and the surface of diaphragm was parallel to the motion direction. This is to avoid the gravity force and the inertia force, due to the system in an unsteady motion, acting on the diaphragm. Another tubing was connected to the '-'ve pressure port and extended to the interior of a 1.5cm-diameter plastic hollow cylinder which was fixed on the backside of the plate. The hollow cylinder was filled with water to about the same water level

in the flume. Because the cylinder's diameter is small, we assume the water surface inside would remain flat during the carriage run. In other words, the reference pressure is a constant. The reason to fix this cylinder to the backside of the plate other than the arbitrary place is to eliminate the force, induced by the water mass subjected to the unsteady motion of the carriage, acting on the diaphragm. The water mass is contained between two openings of the tubings inside the connecting system projected in the moving direction. In so doing, there remains only a minor error which is about 0.1g water inside the pressure hole in the plate. Three accelerations were studied for the pressure measurements: a_1=1.12-1.11t, a_2=0.86-0.88t, and a_3=0.55-0.55t m/sec^2. The experimental results for both free-surface and pressure measurements are presented in the next chapter.

V. RESULTS AND DISCUSSION

The numerical solutions for the free-surface flow generated by a moving plate were calculated by the method stated in Chapter III. A computational domain was taken for x=0~13, and y=0~2, which have been normalized by the unperturbed water depth, with 80x60 grid points. A partial calculation grid system is shown in Figure 12. A coarser and a denser grid system were tested also. The present grid system gives a reasonable accuracy and efficiency. The time increment was controlled that the maximum movement of the plate did not exceed o.2 of the grid spacing in the x-direction at each time step. The calculation at each time step took about 4 CPU minutes in PRIME 9955 minicomputer at the University of Iowa, and took about 9 CPU seconds in CRAY X-MP/48 supercomputer at the University of Illinois at Urbana-Champaign. No vectorization was attempted in the present numerical code when running in the supercomputer. About 20 iterations in each time step were required to obtain an accuracy of 10^{-6} for both velocity and pressure fields.

Chwang (1983) treated the same problem, on the basis of the potential-flow theory, in terms of the small-time-expansions method. The velocity potential was obtained up to and including the third order. An example for the constant acceleration of the plate was presented in his study. For a time-dependent acceleration, $a=a_1+2a_2t$, in the present study, the free-surface profile in the dimensionless form is

$$y^o = 1 + 2\varepsilon^2 \left(1 + \frac{2}{3} a_2^o \right) \sum_{m=1}^{\infty} (k_m h_o)^{-1} e^{-k_m x}, \qquad (V.1)$$

and the normalized hydrodynamic pressure on the plate surface defined in equation (II.5) is

$$p^o = \sum_{m=1}^{\infty} \frac{2 (-1)^{m+1} - 4 a_2^o (-1)^m}{k_m^2 h_o^2} \cos(k_m y)$$

$$+4\varepsilon^2\left[\sum_{m=1}^{\infty}\frac{(-1)^{m+1}}{k_m h_o}\cos(k_m y)\right.$$

$$+\frac{1}{\alpha\pi}\sum_{m=1}^{\infty}(k_m h_o)^{-1}\int_o^{\infty}\frac{k_m\cosh(\xi y)\,d\xi}{(k_m^2+\xi^2)\cosh(\xi h_o)}$$

$$+\frac{4}{\pi}\sum_{m=2}^{\infty}A_m\int_o^{\infty}\frac{\lambda_m\cosh(\xi y)\,d\xi}{(\lambda_m^2+\xi^2)\cosh(\xi h_o)}$$

$$-\left(\sum_{m=1}^{\infty}\frac{(-1)^m}{k_m h_o}\cos(k_m y)\right)^2$$

$$\left.-\left(\sum_{m=1}^{\infty}\frac{(-1)^m}{k_m h_o}\sin(k_m y)\right)^2\right]+O(\varepsilon^4), \qquad (V.2)$$

where h_o denotes the unperturbed fluid depth,

$$\varepsilon^2=\frac{t^2 a_1}{2 h_o}, \qquad a_2^o=\frac{a_2 t}{a_1},$$

$$\alpha=\frac{a_1}{g}, \qquad k_m=\frac{(2m-1)\pi}{2h_o} \quad (m=1,2,\cdots),$$

$$A_m=\sum_{s=1}^{m-1}(h_o^2 k_s k_{m-s})^{-1} \quad (m=2,3,\cdots),$$

$$\lambda_m=\frac{(m-1)\pi}{h_o} \quad (m=2,3,\cdots). \qquad (V.3)$$

The inviscid analytical solution, the viscous numerical results, and the experimental measurements on the free-surface profile and pressure distribution are compared in a series of figures. The free-surface profiles are shown in Figures 13 to 15 for different accelerations at three sequential times, ϵ^2=0.05, 0.1, and 0.15. The agreement between the present numerical results and the experimental measurements is quite satisfactory. The numerical method predicts the water elevation equally well in the region very close to the plate where viscous and surface-tension effects are important. Chwang's theory (1983) gives a good prediction in the region away from the plate and at small time. After a further examination, we found that his theory overpredicts the elevation in the region close to the plate and underpredicts the elevation in the region away from the plate. The larger the time is, the larger the difference would be. This is due to a mathematical singularity, which is predicted by the potential-flow theory, at the intersection of the plate and the free surface. A certain amount of mass is piled on the plate and causes an underprediction of the elevation in the outer region. However, the physical singularity was not observed in the experiments. The water surface simply rises up along the plate during the initial stage of the plate motion. Thereafter, there is a train of waves propagating downstream along the channel. A few pictures showing the initial stage of the plate motion are given in Figures 16 to 18.

A comparison of the pressure distribution on the plate surface is shown in Figures 19 to 21. The numerical method predicts the results quite well. Chwang's theory agrees with the measurements in the region close to the channel bottom and at small time. However, his solution overpredicts the pressure near the free surface and at large time. This is due to the limitation of the small-time-expansions method and a mathematical singularity at the unperturbed free surface. Another reason is that the viscous dissipation is not included in the potential theory.

The time evolution of the velocity vector field is shown in Figures 22 to 24. These figures indicate that the upper portion of water in front of the plate is pushed up and forward. The water near the bottom is pushed forward only. The time evolution of the hydrodynamic pressure field is presented in Figures 25 to 27. The values on the contour lines correspond to the hydrodynamic pressure. These figures indicate that the pressure reaches its maximum values near the corner of

the plate and the channel bottom, as expected from physical intuition. Note also that the values of the pressure decrease vertically from channel bottom to free surface. The pressure contour lines also show that a pressure wave propagates downstream as time increases.

VI. CONCLUSIONS

The physical problem of the free-surface flow generated by an impulsively accelerating, surface-piercing, vertical plate has been studied numerically as well as experimentally. The unsteady, two-dimensional Navier-Stokes equations are solved numerically to describe the flow phenomena. The continuity equation and two dynamic boundary conditions on normal and tangential stresses at the free surface are applied to determine the pressure and two velocity components at the free surface. The kinematic boundary condition provides the movement of the free surface. A series of experiments has been conducted in an open channel with a constant water depth. The free-surface profile in front of the plate and the pressure distribution on the plate surface are measured.

The inviscid analytic solution, the viscous numerical results, and the experimental measurements have been compared. The agreement of the free-surface profile between the numerical results and the experimental measurements is fairly good. The inviscid analytical solution developed by Chwang (1983) also gives a good prediction in the region away from the plate and at small time. The agreement of the pressure distribution on the plate surface between the numerical and experimental results is also satisfactory. Chwang's theory agrees with the experimental measurements quite well in the vicinity of the channel bottom and at small time. The mathematical singularity, which is predicted by the potential-flow theory, at the intersection of the plate and the free surface is not observed in the physical experiments. The water surface simply rises up ahead of the plate during the initial stage of the plate motion.

In the present study, the carriage is released manually and driven by a freely falling weight bucket. All the measurements are taken within a small time after releasing the carriage. It is important to require the acceleration be a step function at time $t=0_+$. Although the output data were carefully checked, the human error still exists. To improve the accuracy, the carriage could be driven by an electrically controlled motor system from which the rate of acceleration can be regulated. For the pressure measurements, the measuring range is about 9~20% of the capacity of

the pressure transducer in the present experiments. The degree of accuracy can be improved by using a pressure transducer with more compatible capacity.

The present numerical code has been verified by the experimental measurements and can predict satisfactorily the flow field generated by the impulsive motion of a plate. This two-dimensional numerical code can be extended to study similar problems on axisymmetric or three-dimensional flows. For the flow domain with a complex configuration, the numerically-generated boundary-fitted coordinate system can be used, which not only fits the body boundary but also fits the free-surface boundary.

REFERENCES

Chan, R.K.C. and Street, R.L., "SUMMAC- A Numerical Model for Water Waves", Technical Report No.135, 1970, Dept. of Civil Eng., Stanford University.

Chan, R.K.C. and Street.R.L., "A Computer Study of Finite- Amplitude Water Waves", J. Comp. Phys., Vol.6, 1970, pp.68-94.

Chen, C.J. and Others, "The Finite Analytic Method", Iowa Institute of Hydraulic Research, University of Iowa, IIHR Report 232, 1980-1986, Vol.1-7, Iowa City.

Chen, H.C. and Patel, V.C., "Laminar Flow at the Trailing Edge of a Flat Plate", AIAA J., Vol.25, No.7, 1987, pp.920-928.

Chwang, A.T., "Nonlinear Hydrodynamic Pressure on an Accelerating Plate", Physics of Fluids, Vol.26, 1983, pp.383-387.

Durbin, D.A., "Considerations on the Moving Contact-Line Singularity, with Application to Frictional Drag on a Slender Drop", J. Fluid Mech., Vol.197, 1988, pp.157-169.

Dussan, V., E.B., "The Moving Contact Line: the Slip Boundary Condition", J. Fluid Mech., Vol.77, 1976, pp.665-684.

Faltinsen, O.M., "Numerical Solution of Transient Nonlinear Free- Surface Motion Outside or Inside Moving Bodies", Second International Conference on Numerical Ship Hydrodynamics, U.C. Berkeley, 1977, pp.347-357.

Frederiksen, C.S. and Watts A.M., "Finite-Element Method for Time-Dependent Incompressible Free-Surface Flow", J. Comp. Phys., Vol.39, 1981, pp.282-304.

Greenhow, M. and Lin, W.M., "Nonlinear Free Surface Effects: Experiments and Theory", Report No.83-19, Dept. of Ocean Eng., Massachusetts Institute of Technology, 1983.

Hirt, C.W., Cook, J.L., and Butler, T.D., "A Lagrangian Method for Calculating the Dynamics of an Incompressible Fluid with Free Surface", J. Comp. Phys., Vol.5, 1970, pp.103-124.

Hirt, C.W. and Shannon, J.P., "Free-Surface Stress Condition for Incompressible Flow Calculations", J. Comp. Phys., Vol.2, 1968, pp.403-411.

Hocking, L.M., "A Moving Fluid Interface on a Rough Surface", J. Fluid Mech., Vol.76, 1976, pp.801-817.

Kawahara, M. and Miwa, T., "Finite-Element Analysis of Wave Motion", International Journal for Numerical Methods in Engineering, Vol.120, 1984, pp.1193-1210.

Lamb,H., "Hydrodynamics", 1932, Dover.

Lin, W.M., Newman, J.N., and Yue, D.K., "Nonlinear Forced Motions of Floating Bodies", Fifteenth Symp. on Naval Hydrodynamics, 1984, pp.1-15.

Masuko, A., Miyata, H., and Kajitani, H., "Numerical Analysis of Free Surface Shock Waves Around Bow by Modified MAC Method (2nd Report)",J. Soc. Nav. Archit. Jpn., Vol.152, 1982, pp.1- 12.

Miyata, H. and Inui, T., "Nonlinear Ship Waves", Advances in Applied Mechanics, Vol.24, 1984, pp.215-288.

Miyata, H. and Nishimura, S., "Finite-Difference Simulation of Nonlinear Ship Waves", J. Fluid Mech., Vol.157, 1985, pp.325- 357.

Miyata, H., Nishimura, S., and Masuko, A., "Finite Difference Simulation of Nonlinear Waves Generated by Arbitrary Three- Dimensional Configuration", J. Comp. Phys., Vol.60, 1985, pp.391-436.

Miyata, H., Sato, T., and Baba, N., "Difference Solution of a Viscous Flow with Free-Surface Wave about an Advancing Ship", J. Comp. Phys., Vol.72, 1987, pp.393-421.

Nicols, B.D. and Hirt, C.W., "Improved Free Surface Boundary Conditions for Numerical Incompressible Flow Calculations", J. Comp. Phys., Vol.8, 1971, pp.434-448.

Nickell, R.E., Tanner, R.I., and Caswell, B., "The Solution of Viscous Incompressible Jet and Free-surface Flows Using Finite-Element Methods", J. Fluid Mech., Vol.65, 1974, pp.189-206.

Patankar, S.V., "Numerical Heat Transfer and Fluid Flow", 1980, McGraw-Hill.

Patankar, S.V., "A Calculation Procedure for Two-Dimensional Elliptic Situations", Numerical Heat Transfer, Vol.4, 1981, pp.409-425.

Pearlman, M.D., "Dynamic Calibration of Wave Probes", M.I.T. Contract No. DSR 6913, Dept. of Naval Architecture and Marine Eng., Massachusetts Institute of Technology, 1963.

Reddy, K.R. and Tanner, R.I., "Finite-Element Solution of Viscous Jet Flows with Surface Tension", Computers and Fluids, Vol.6, 1978, pp.83-91.

Richmond, M.C., "Surface Curvature and Pressure Effects on Transient Flow: An Assessment Based on Numerical Solution of the Reynolds Equations", Ph.D. Dissertation, Univ. of Iowa, Dept. of Civil and Environmental Eng., Iowa City, Iowa, 1987.

Ramaswamy, B. and Kawahara, M., "Lagrangian Finite Element Analysis Applied to Viscous Free Surface Fluid Flow", International Journal for Numerical Methods in Fluids. Vol.7, 1987, pp.953-984.

Ramaswamy, B. and Kawahara, M., "Arbitrary Lagrangian Eulerian Finite Element Method for Unsteady, Convective, Incompressible Viscous Free Surface Fluid Flow", International Journal for Numerical Method in Fluids, Vol.7, 1987, pp.1053-1075.

Roberts, A.J., "Transients Free-Surface Flows Generated by a Moving Vertical Plate", Q. J. Mech. Appl. Math., Vol.40, Pt.1, 1987, pp.129-158.

Suzuki, A., Miyata, H., and Kanai, M., "Numerical Analysis of Free Surface Shock Waves Around Bow by Modified MAC Method (1st Report)", J. Soc. Nav. Archi. Jpn., Vol.150, 1981, pp.1-8.

Tang, C.J., "Free-Surface Flow Phenomena Ahead of a Two-Dimensional Body in a Viscous Fluid", Ph.D. Dissertation, Dept. of Mech. Eng., Univ. of Iowa, Iowa City, Iowa, 1987.

Viecelli, J.A., "A Computing Method for Incompressible Flow Bounded by Moving Walls", J. Comp. Phys., Vol.8, 1971, pp.119- 143.

Wang, K.H., "Nonlinear Impulsive Motion of a Vertical Cylinder", Ph.D. Dissertation, Univ. of Iowa, Dept.of Mech. Eng , Iowa City,Iowa, 1985.

Welch, J.E., Harlow, F.H., Shannon, J.P., and Daly, B.J., "The MAC Method: A Computing Technique for Solving Viscous, Incompressible, Transient Fluid Flow Problem Involving Free Surface", Report No. LA-3425, 1965, Los Alamos Scientific Laboratory.

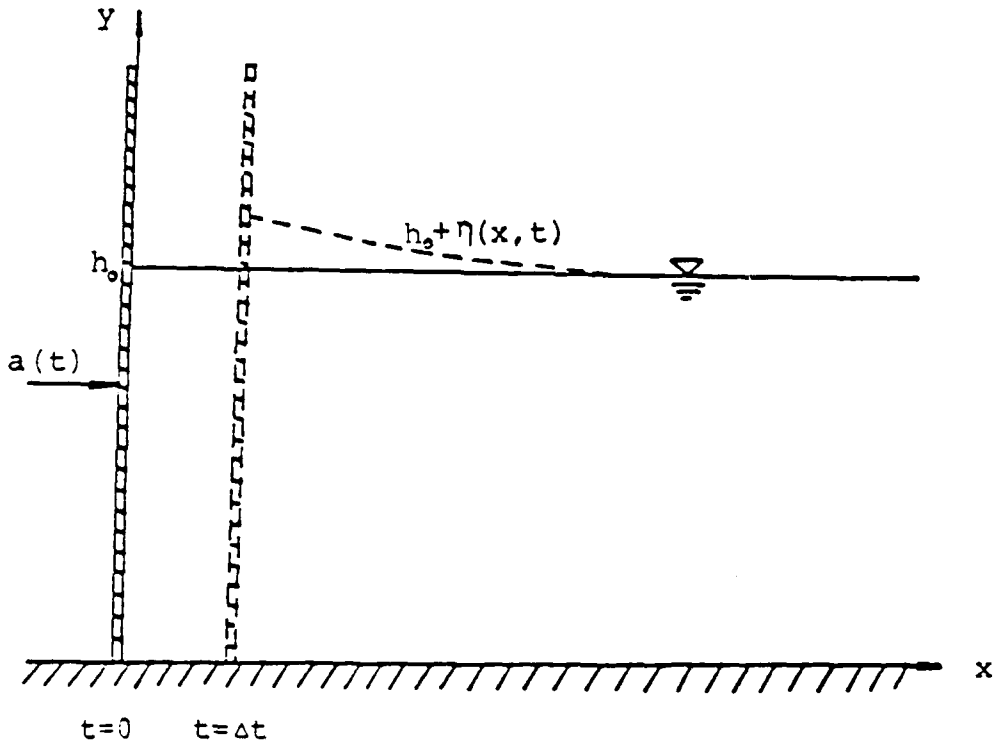

Figure 1. Schematic diagram of an accelerating plate.

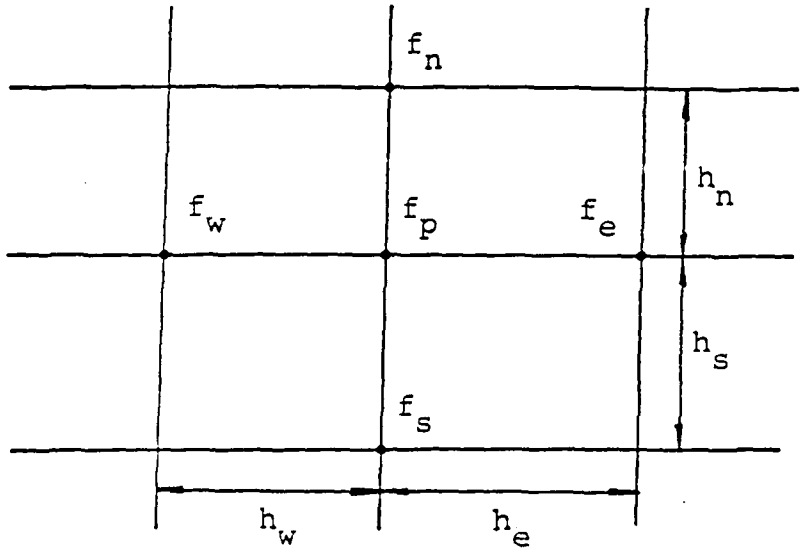

Figure 2(a). Numerical grids.

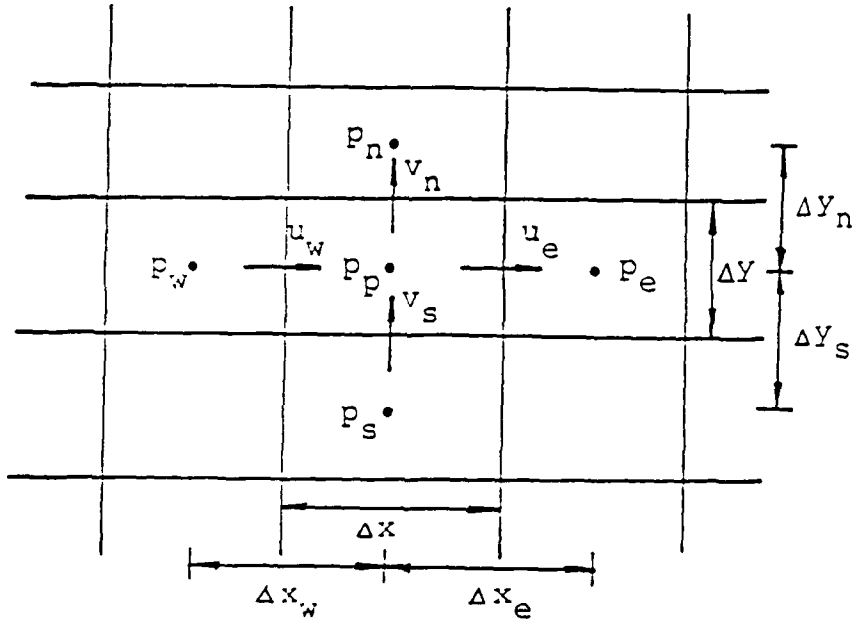

Figure 2(b). Staggered grid system.

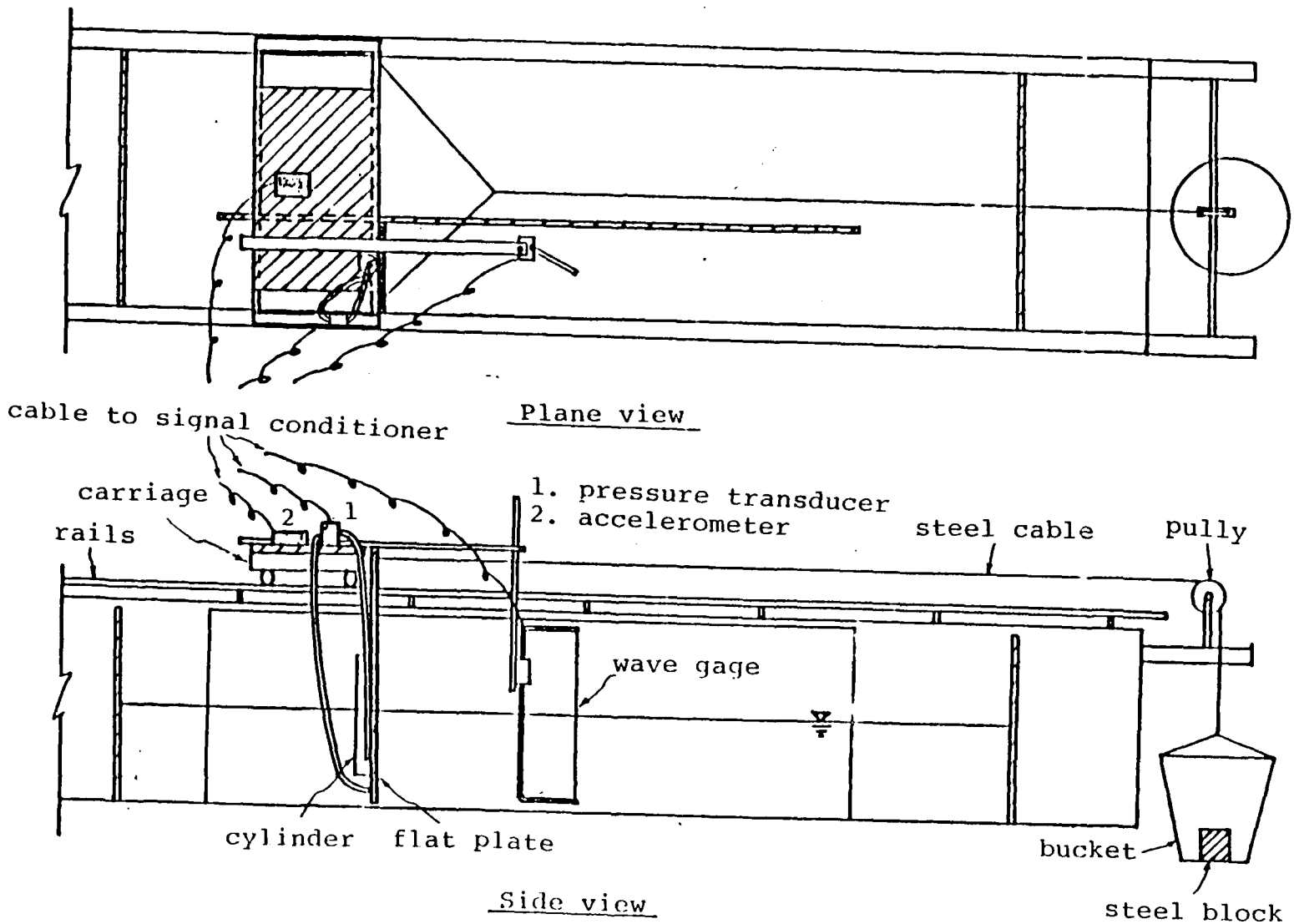

Figure 3. Schematic sketch of the experimental setup.

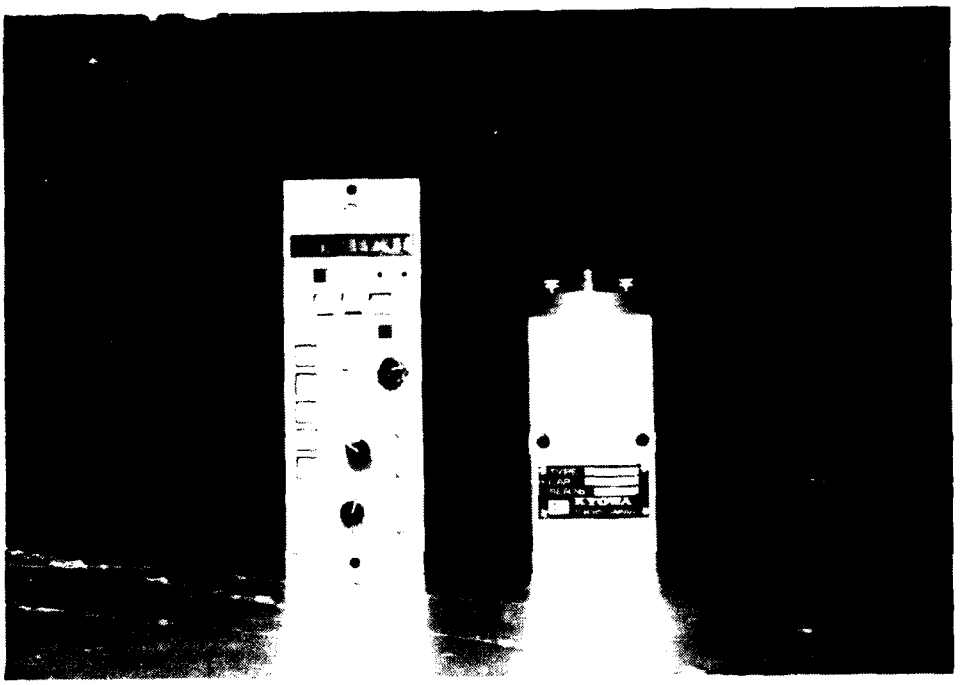

Figure 4. The accelerometer (right) and the signal conditioner.

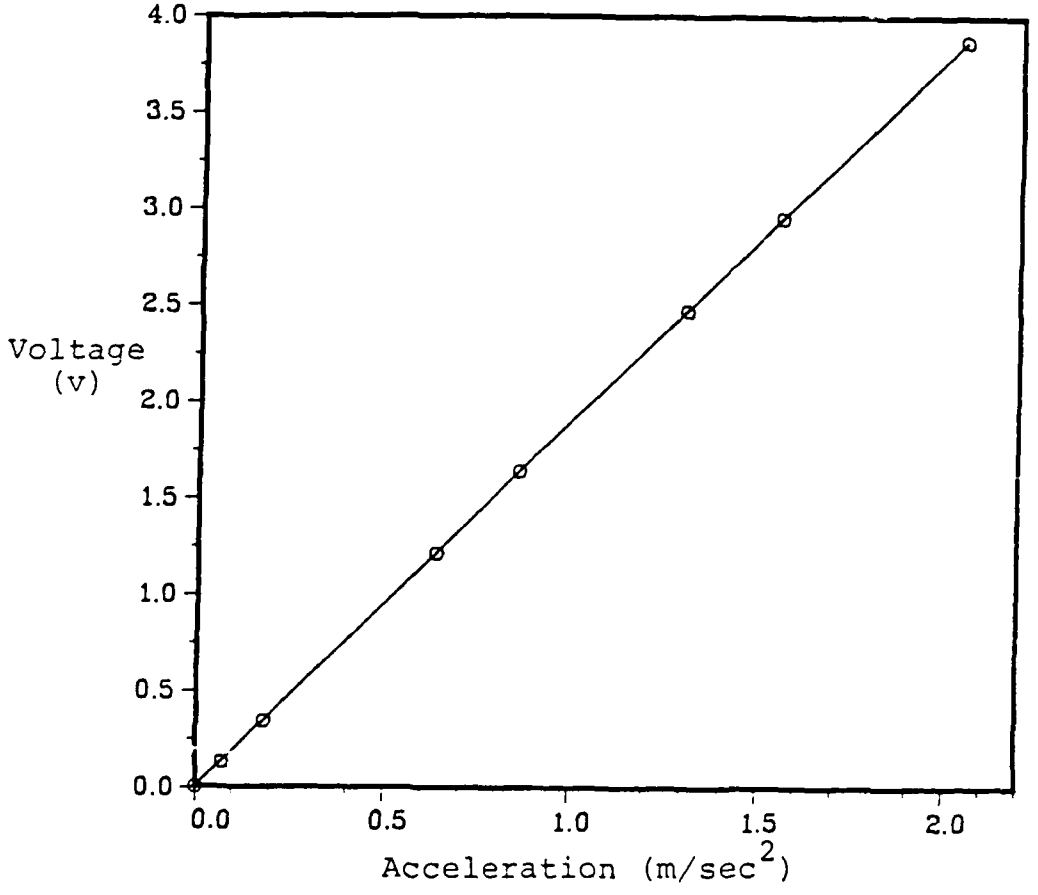

Figure 5. Calibration curve for the accelerometer.

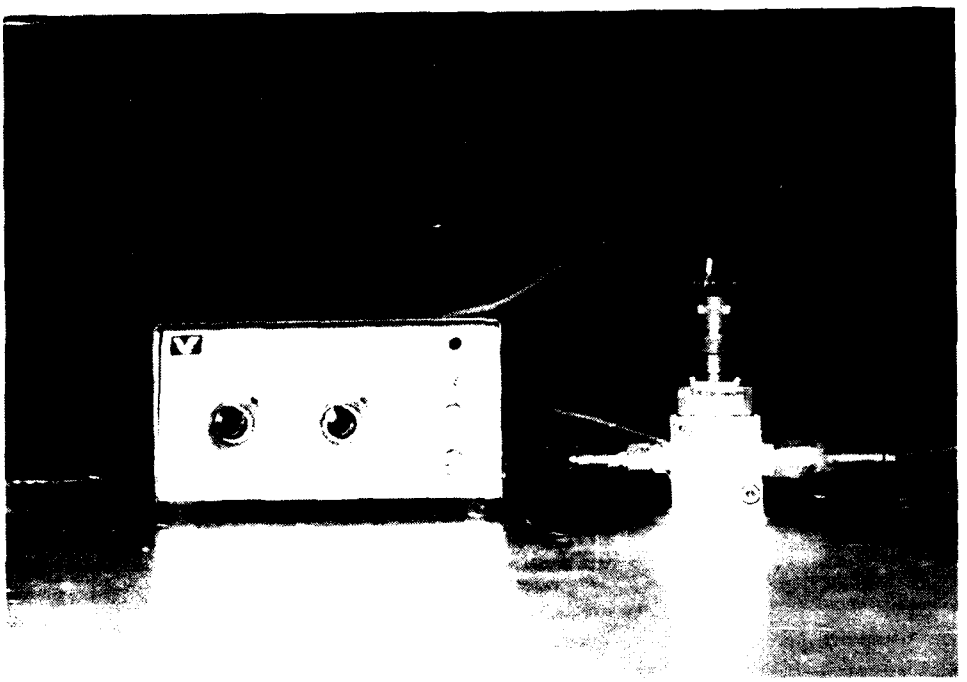

Figure 6. The pressure transducer (right) and the signal conditioner.

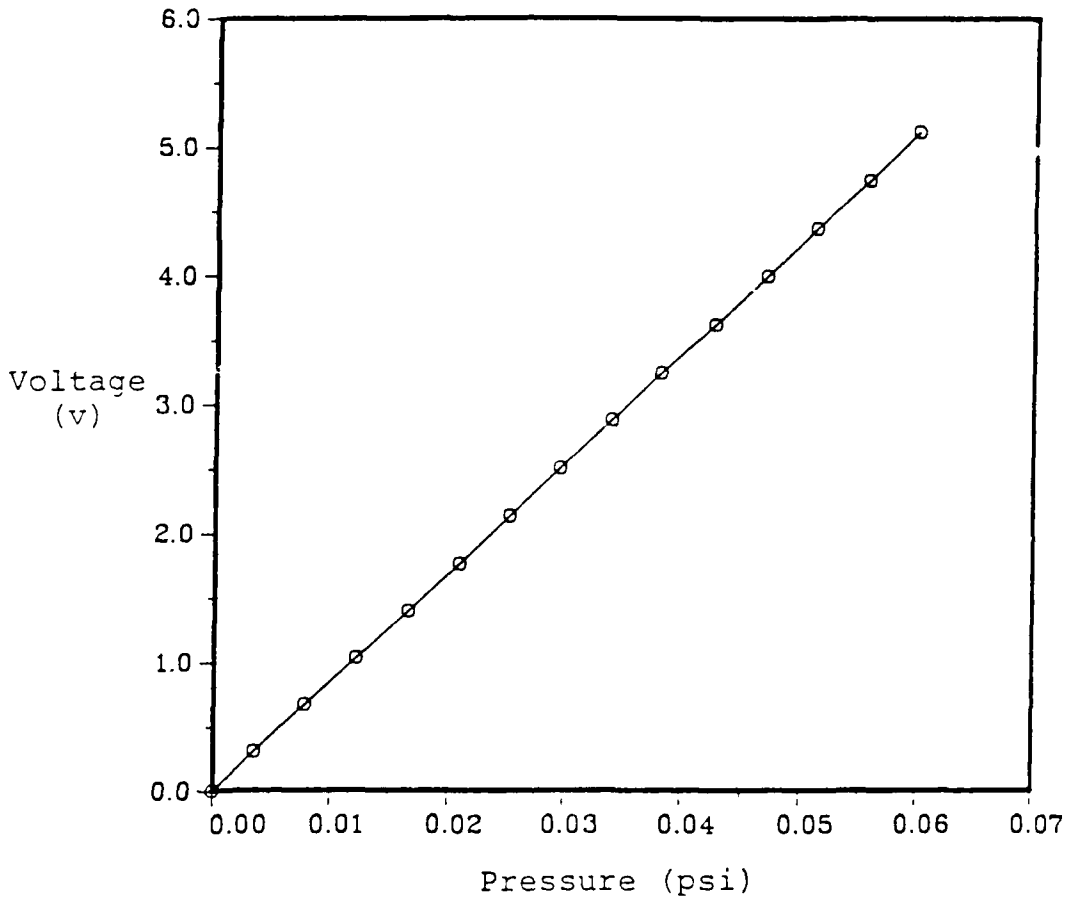

Figure 7. Calibration curve for the pressure transducer.

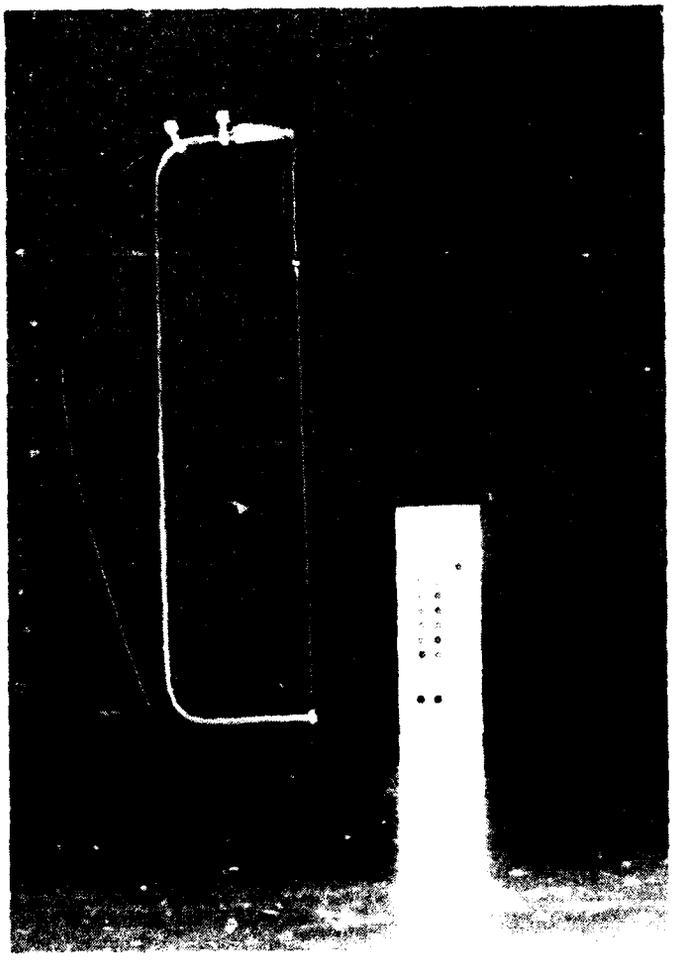

Figure 8. The wave gauge (left) and the signal conditioner.

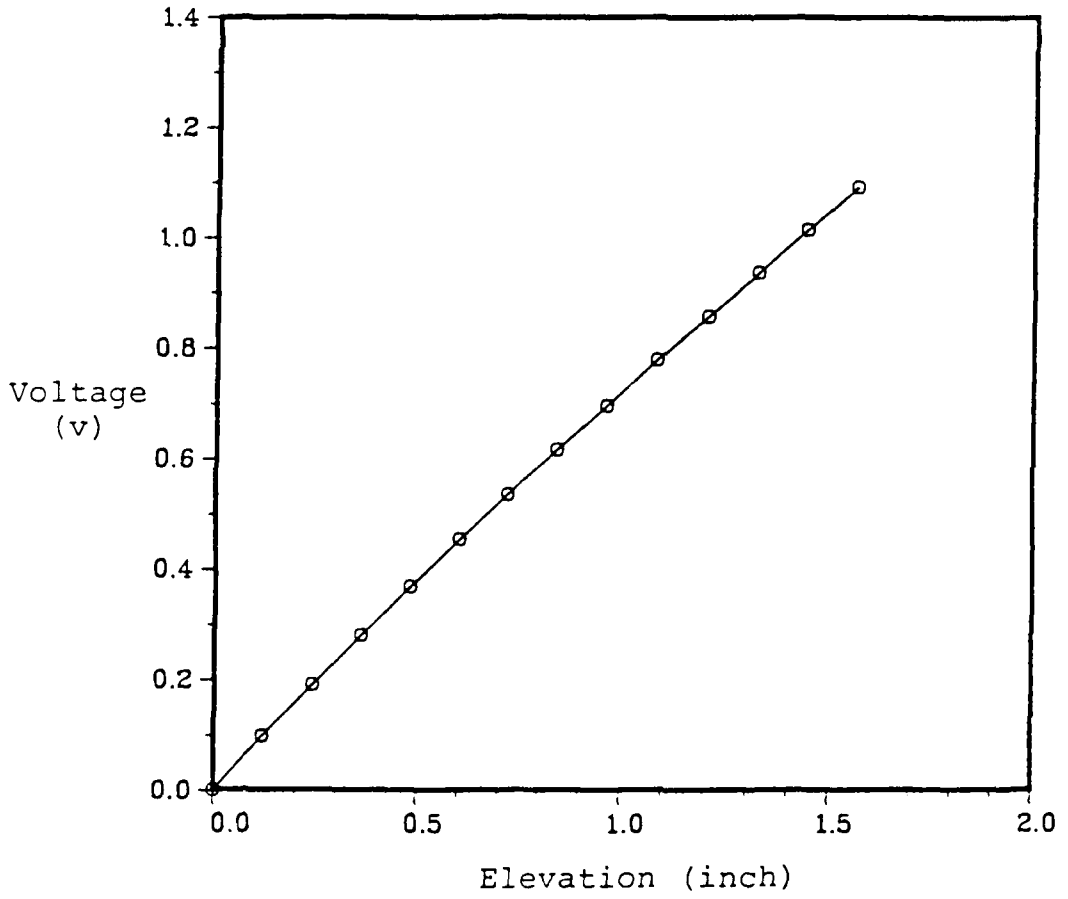

Figure 9. Calibration curve for the wave gauge.

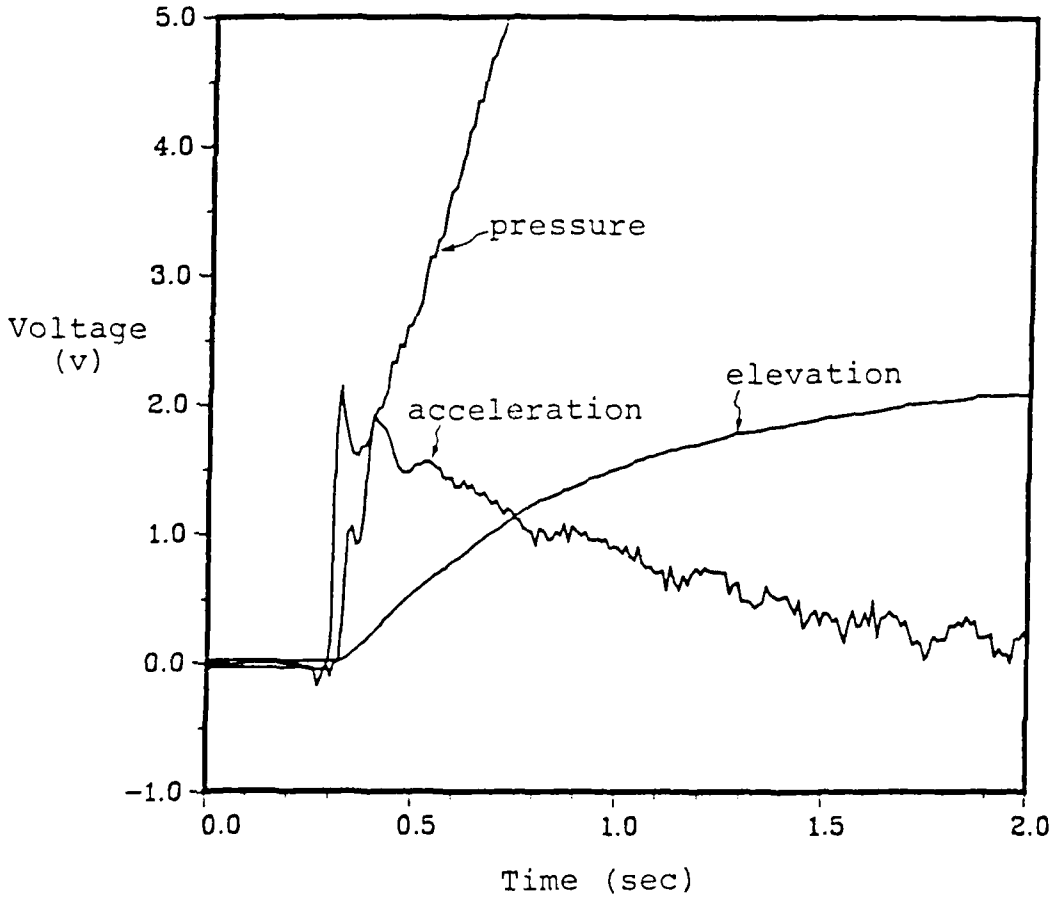

Figure 10. Typical response voltage outputs for acceleration, pressure, and elevation.

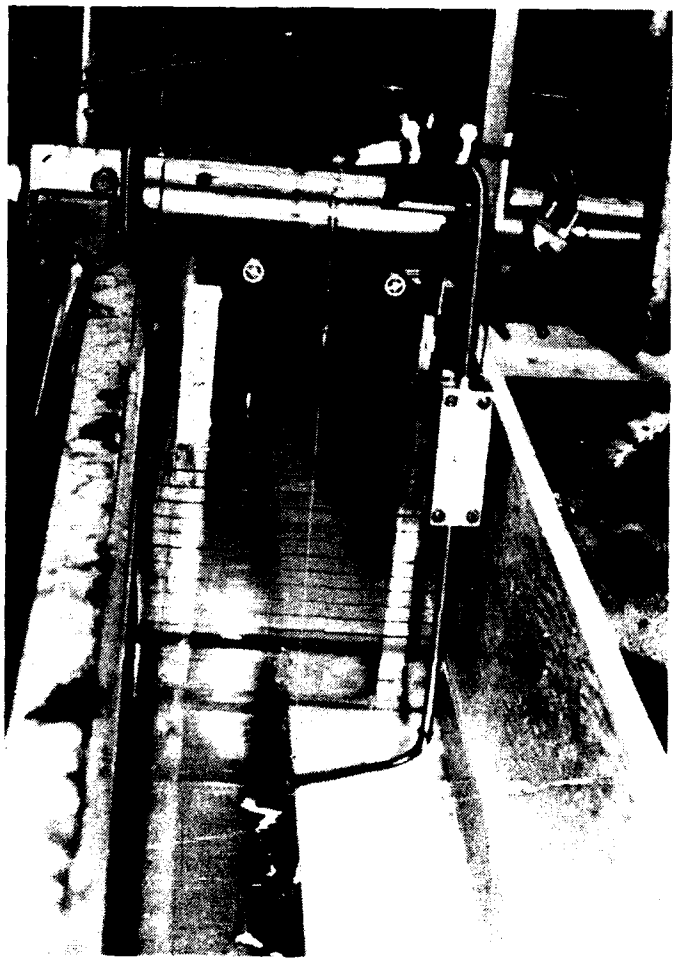

Figure 11. Wave-gauge mounted system.

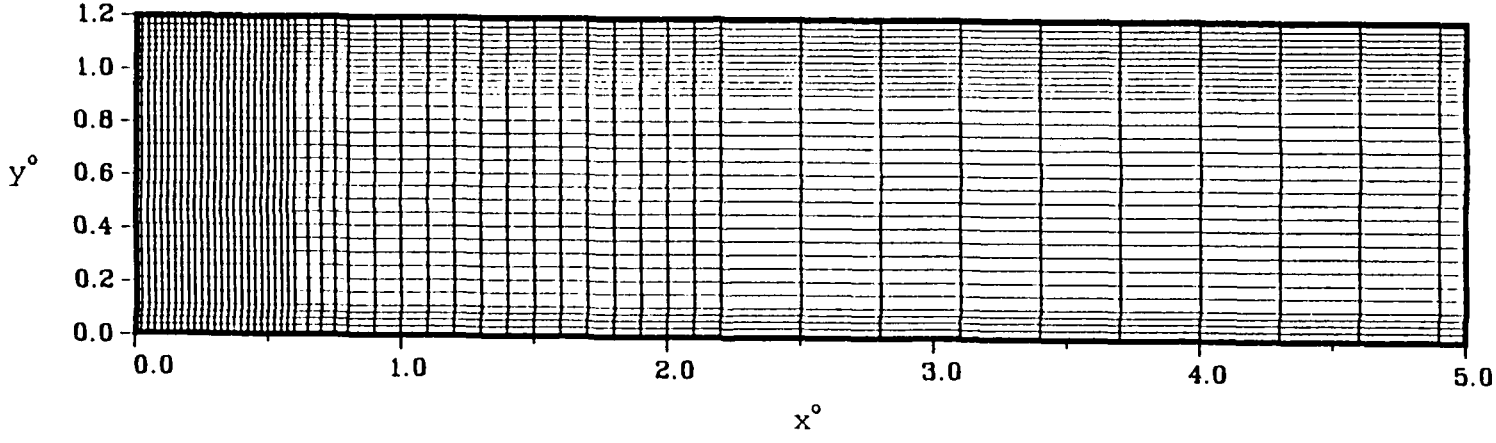

Figure 12. Numerical grids for calculating the nonlinear waves ahead of a plate.

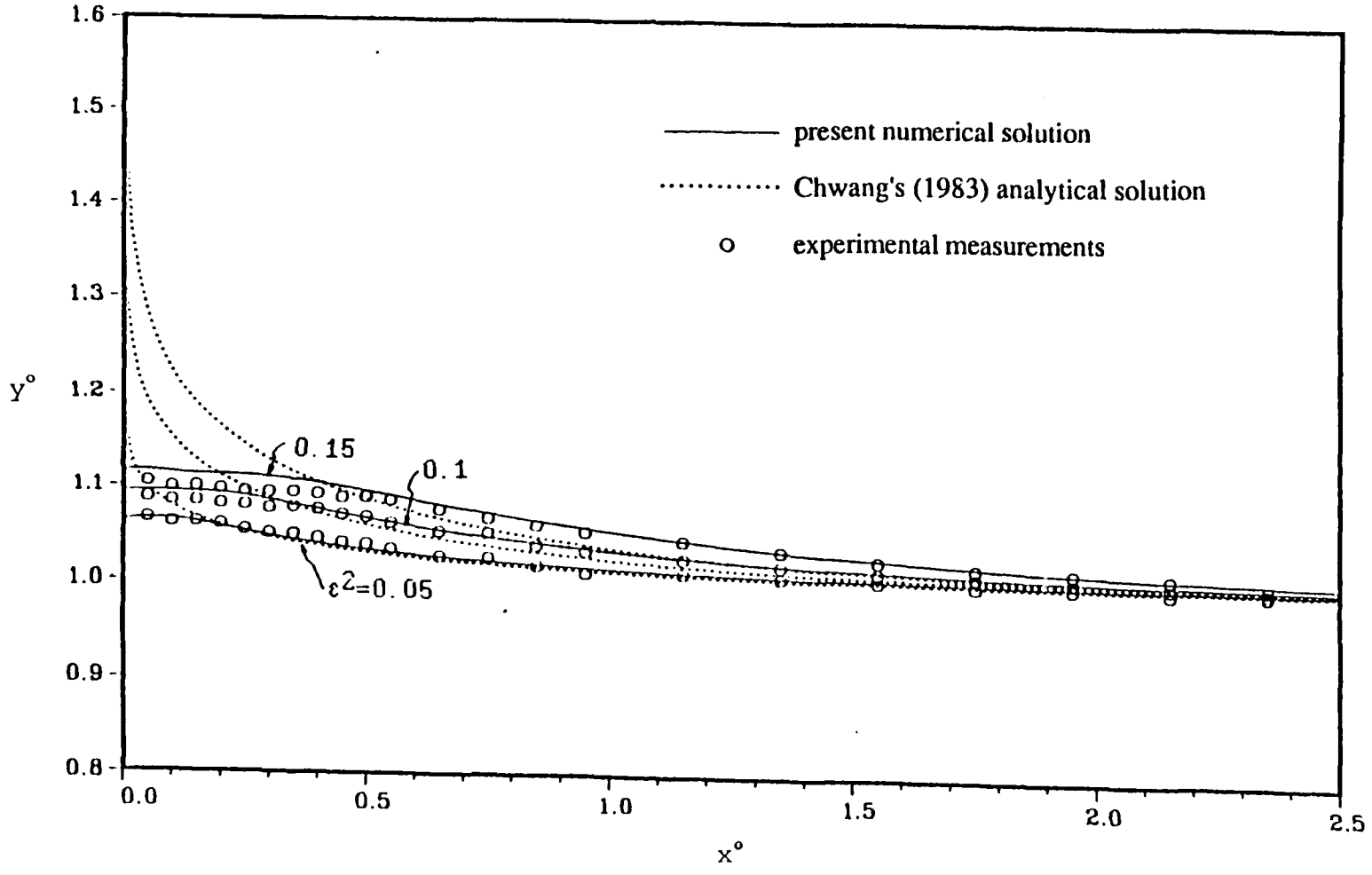

Figure 13. Free-surface profiles for different values of time and a=0.50-0.44t (m/sec^2).

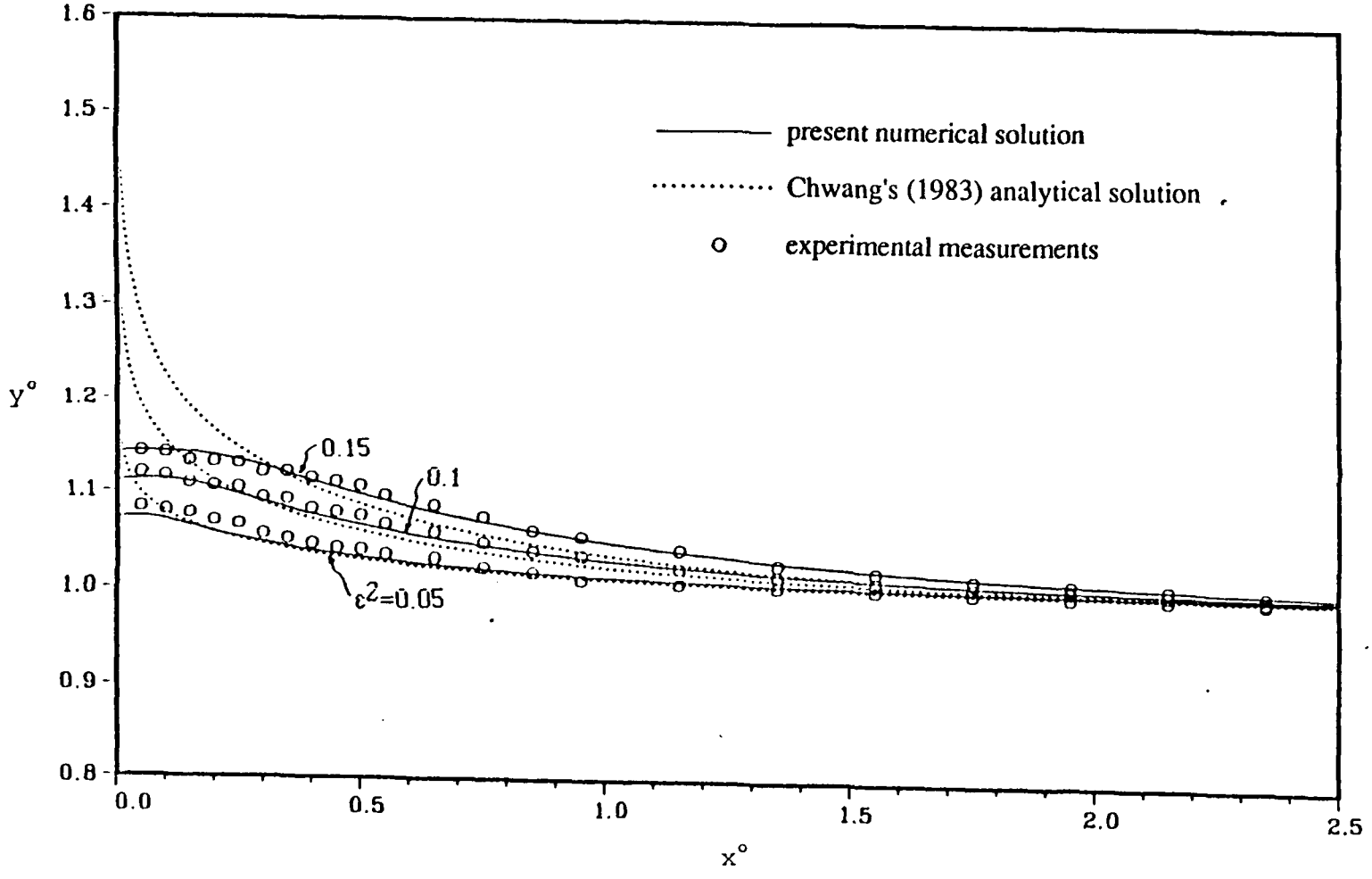

Figure 14. Free-surface profiles for different values of time and a=0.78-0.69t (m/sec^2).

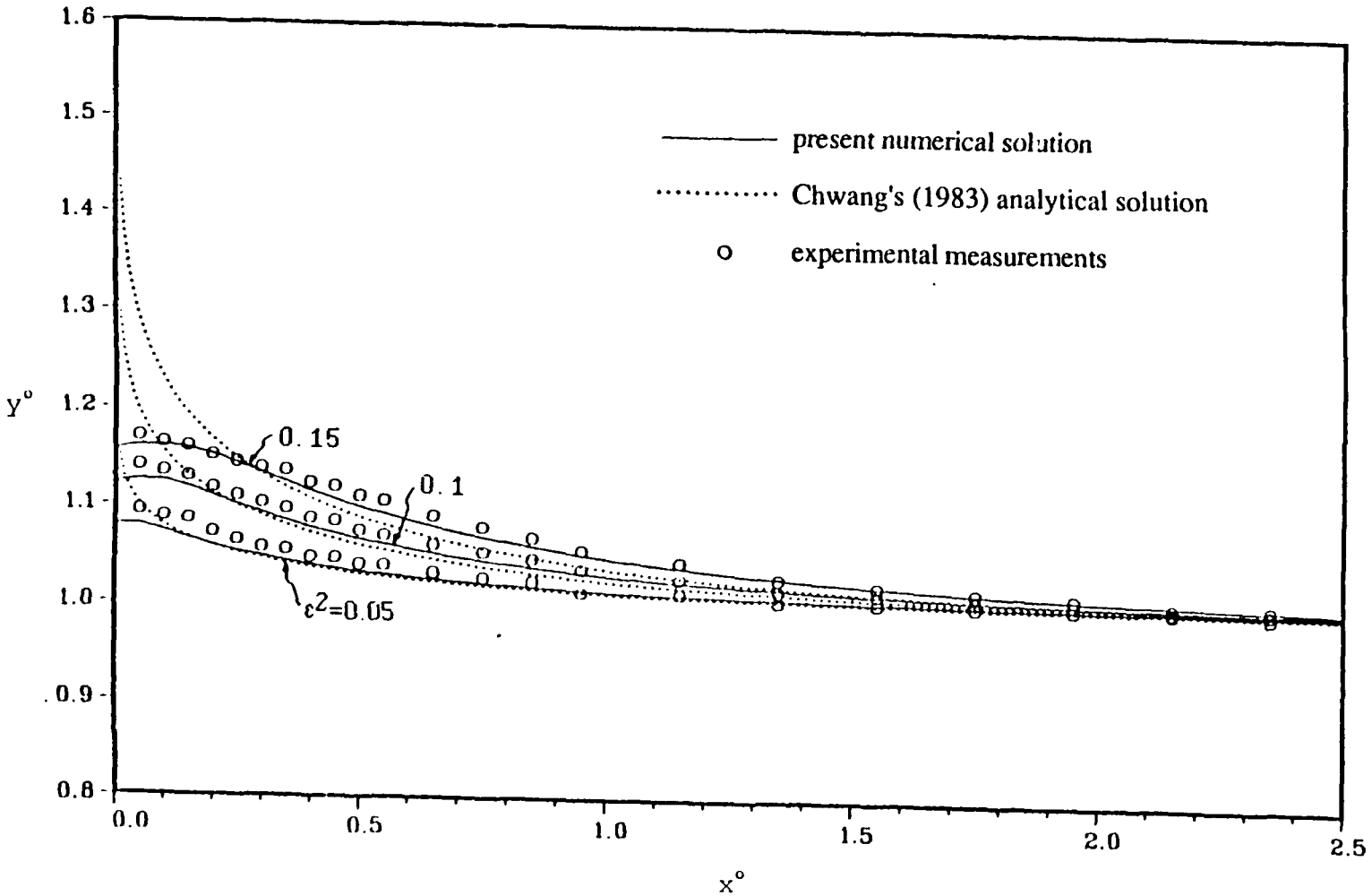

Figure 15. Free-surface profiles for different values of time and a=1.04-0.96t (m/sec^2).

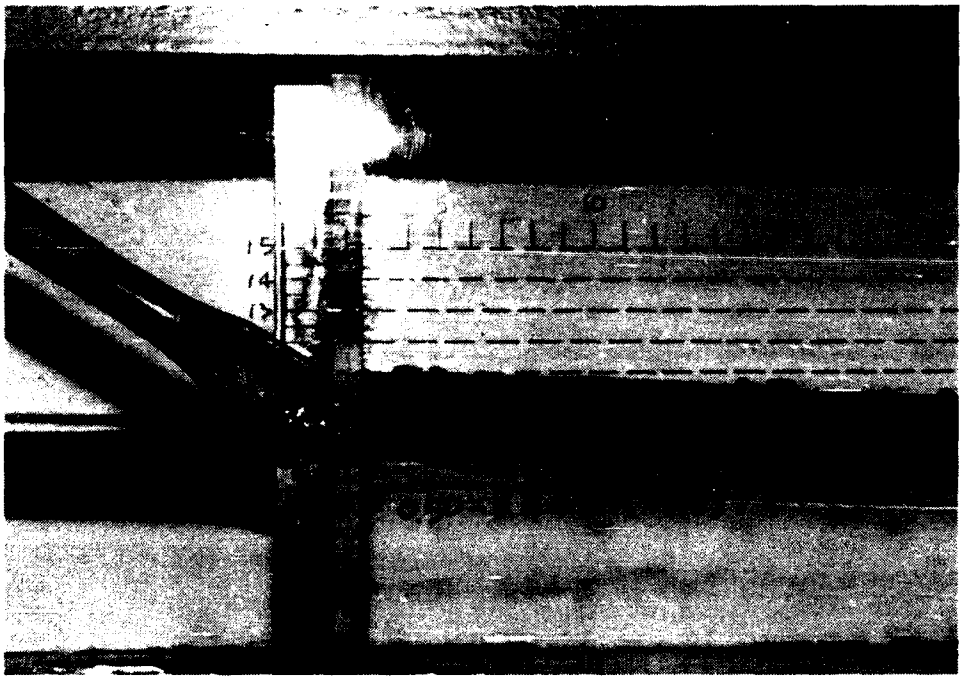

Figure 16. Free-surface profile for a=0.50-0.44t (m/sec^2).

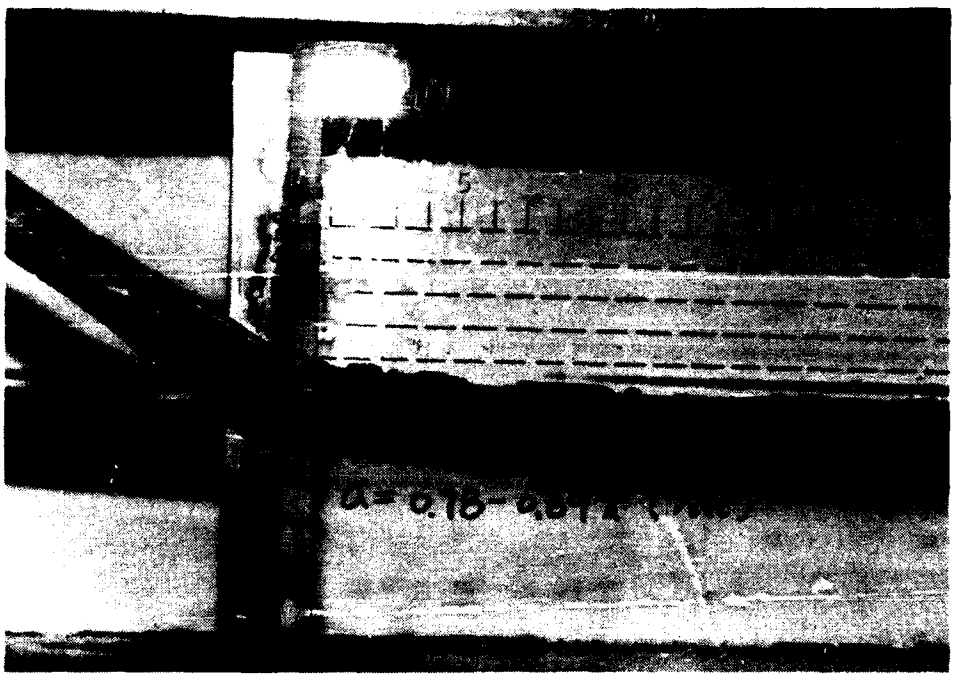

Figure 17. Free-surface profile for a=0.78-0.69t (m/sec^2).

Figure 18. Free-surface profile for $a=1.04-0.96t$ (m/sec^2).

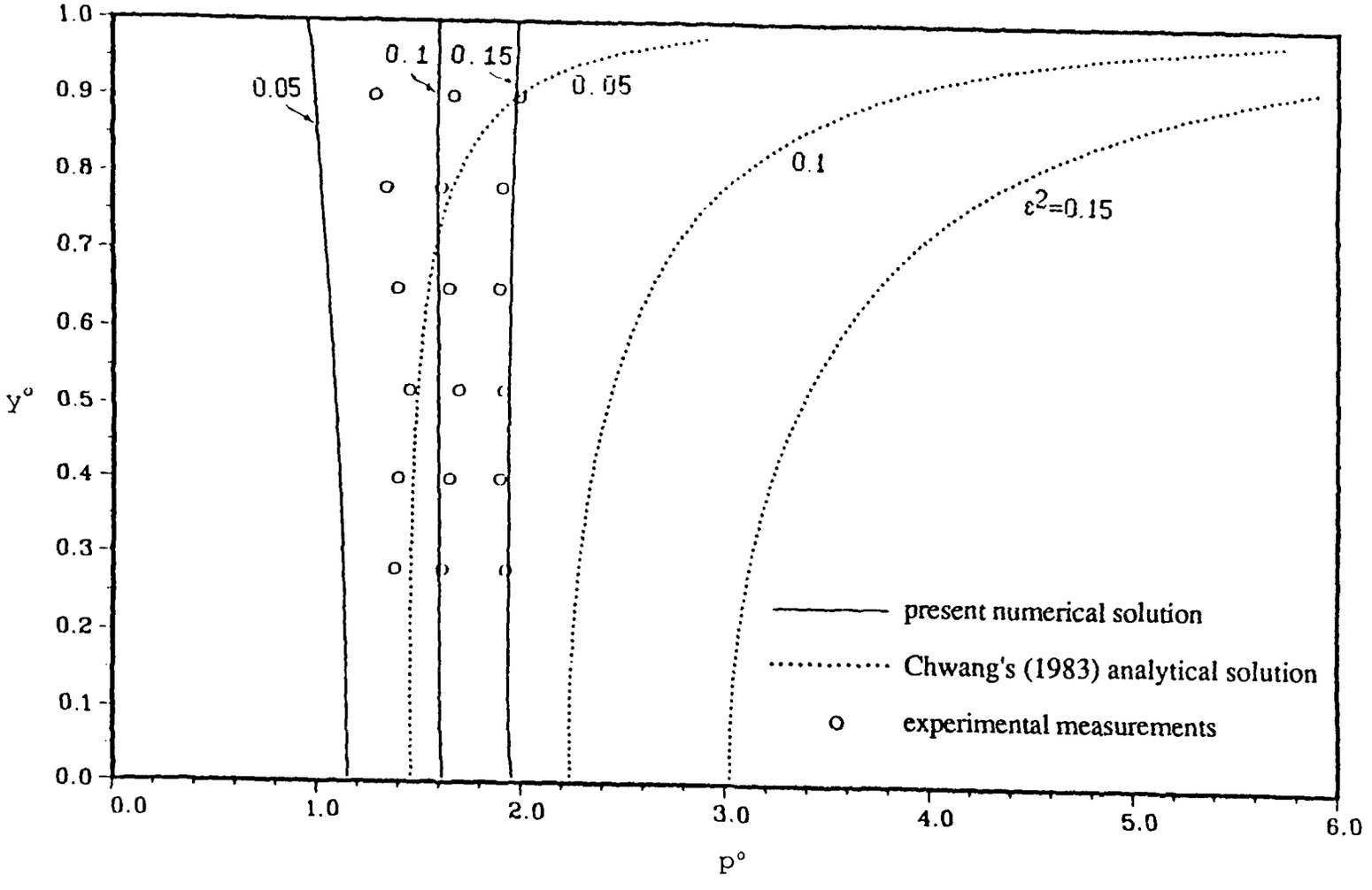

Figure 19. Pressure distribution on the plate surface for different values of time and a=0.55-0.55t (m/sec^2).

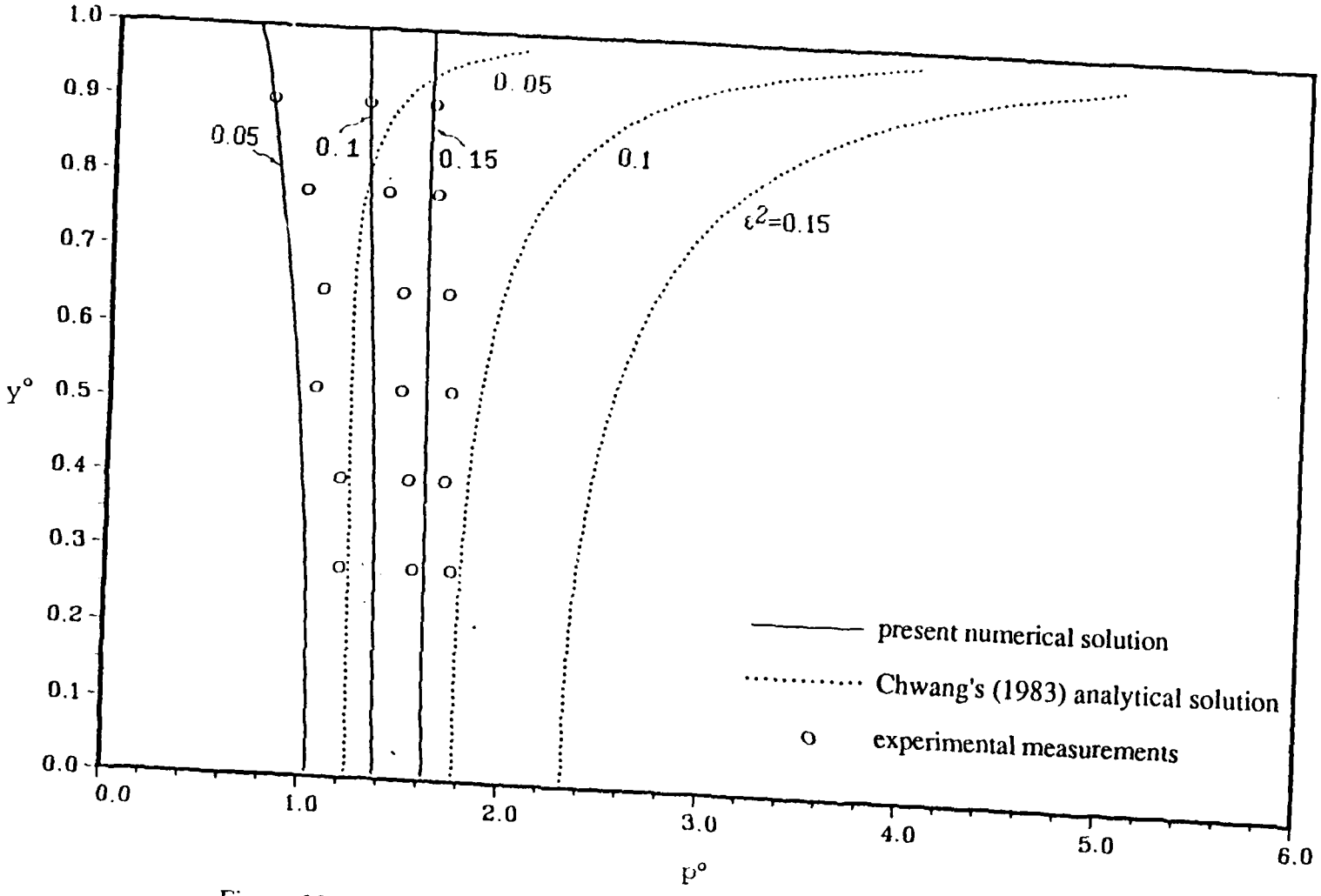

Figure 20. Pressure distribution on the plate surface for different values of time and a=0.86-0.88t (m/sec^2).

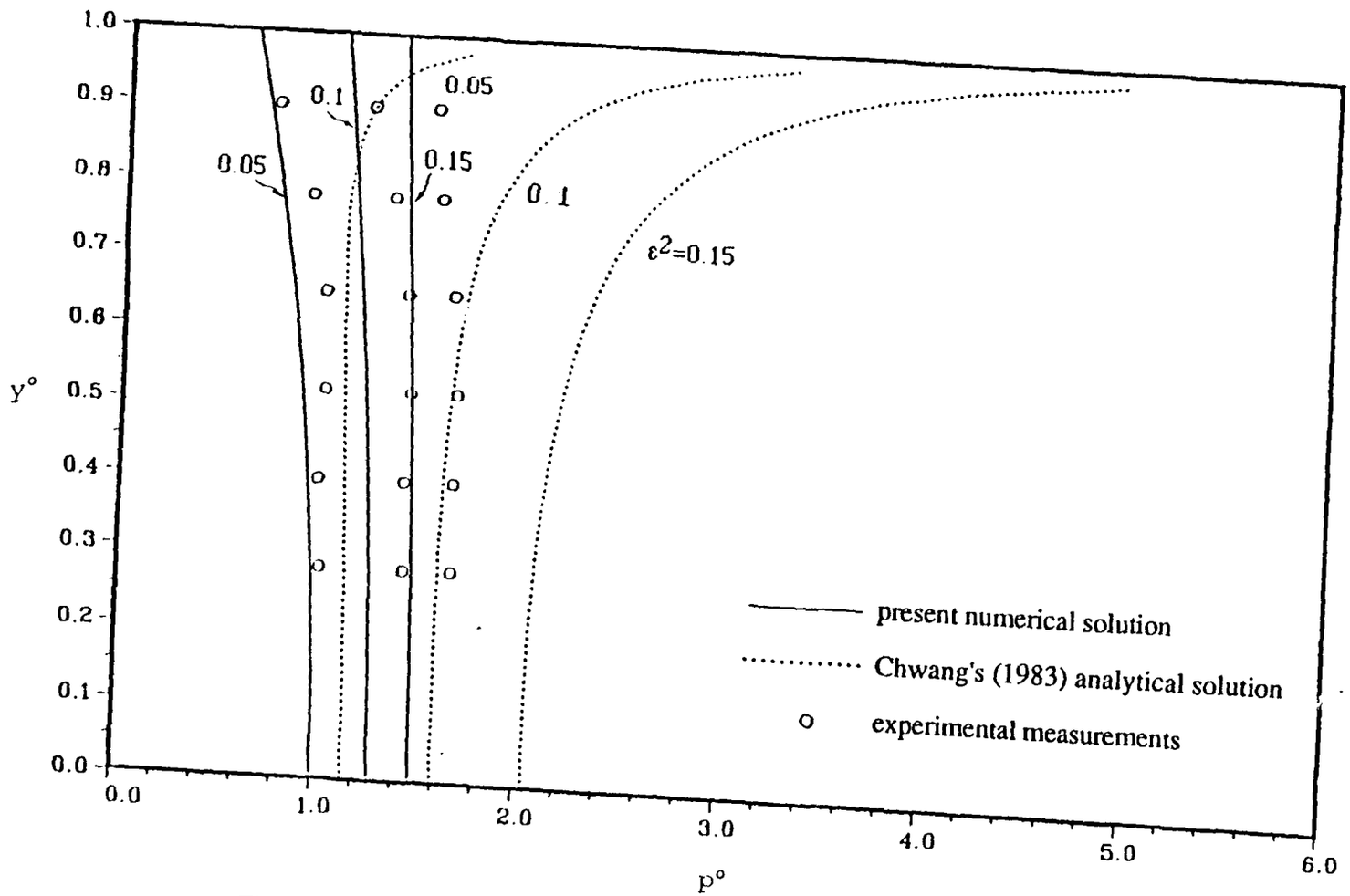

Figure 21. Pressure distribution on the plate surface for different values of time and a=1.12-1.11t (m/sec^2).

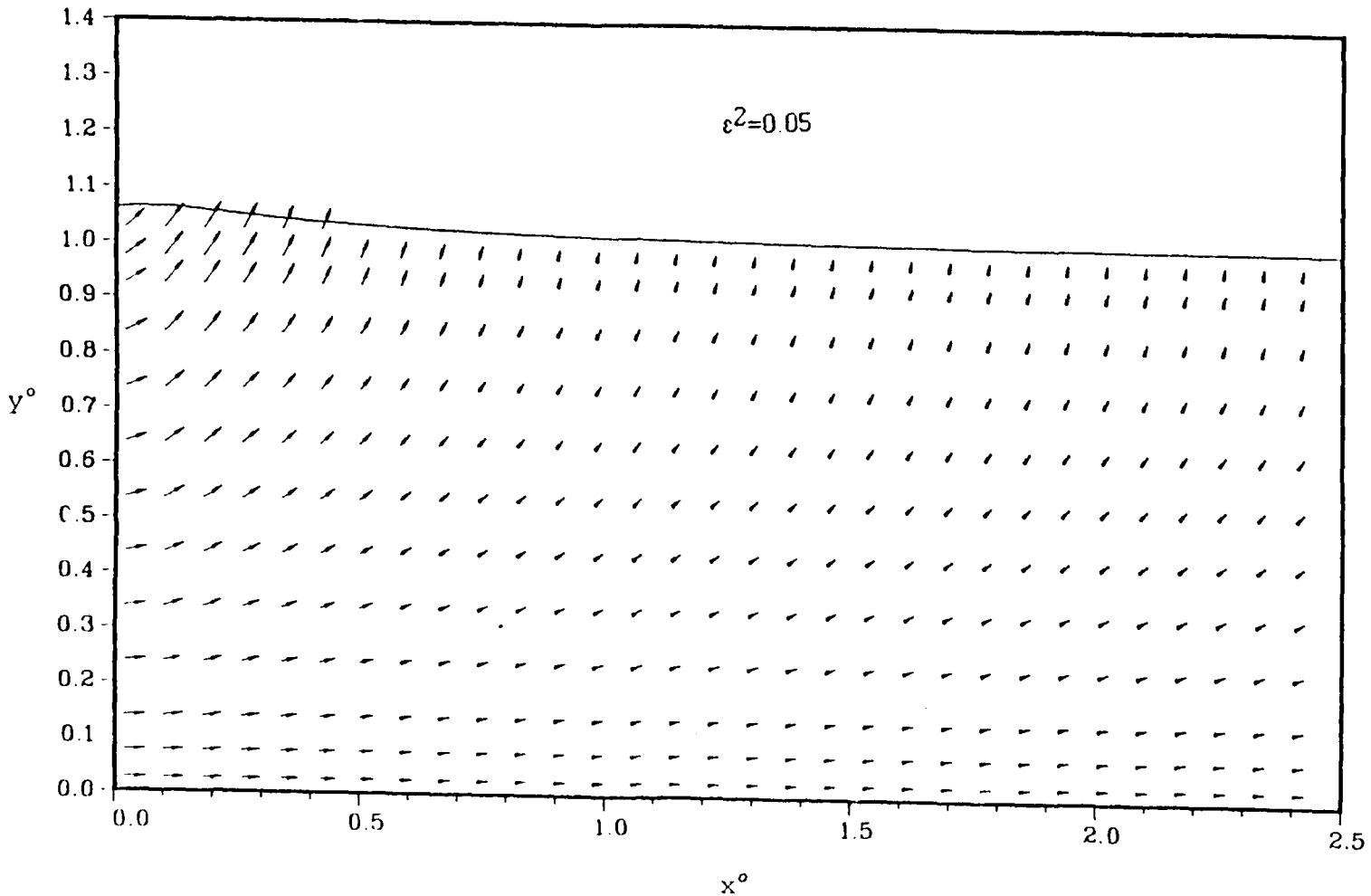

Figure 22. Time evolution of the velocity vector field ahead of the plate for a=0.50-0.44t (m/sec^2).

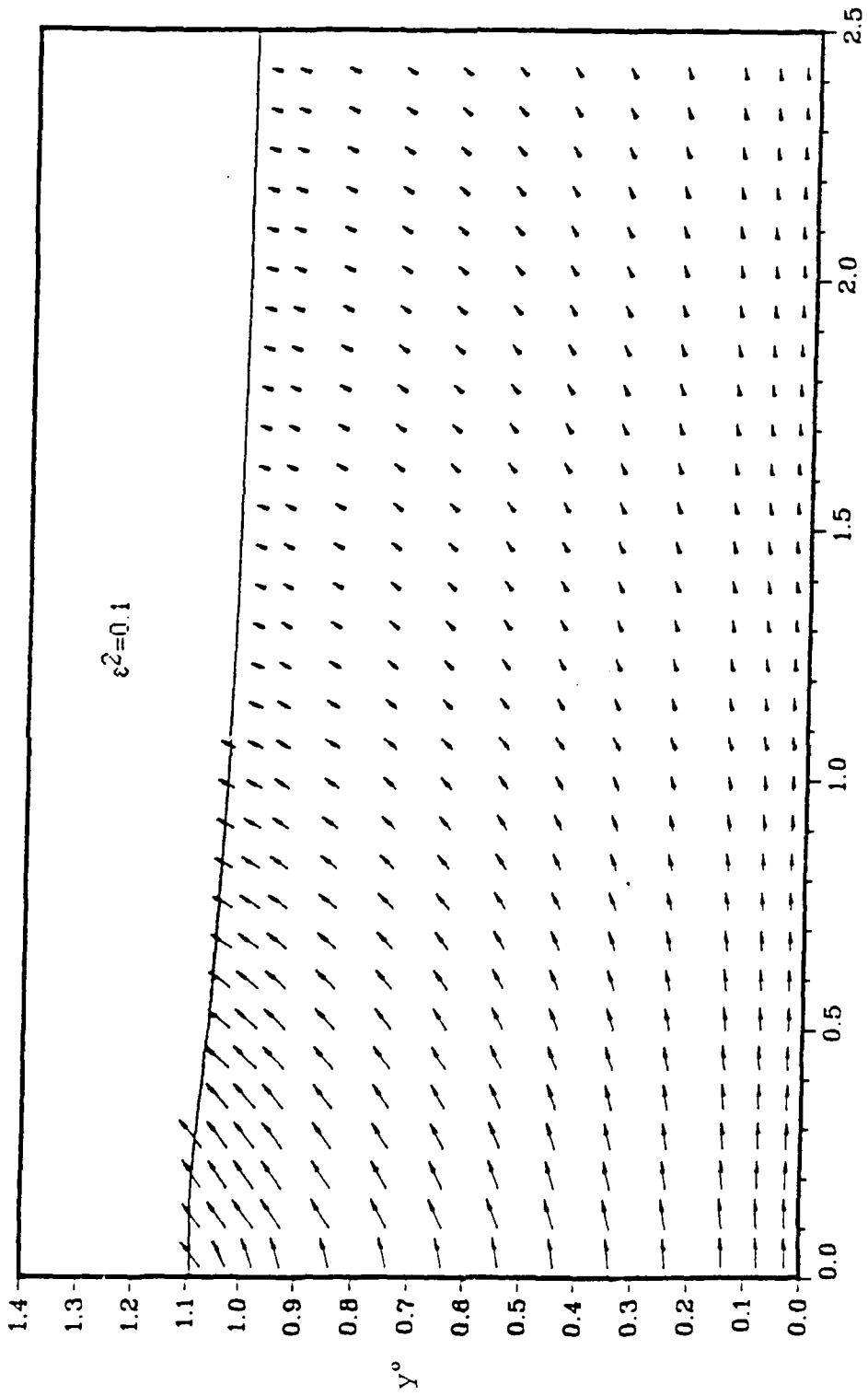

Figure 22. -- continued

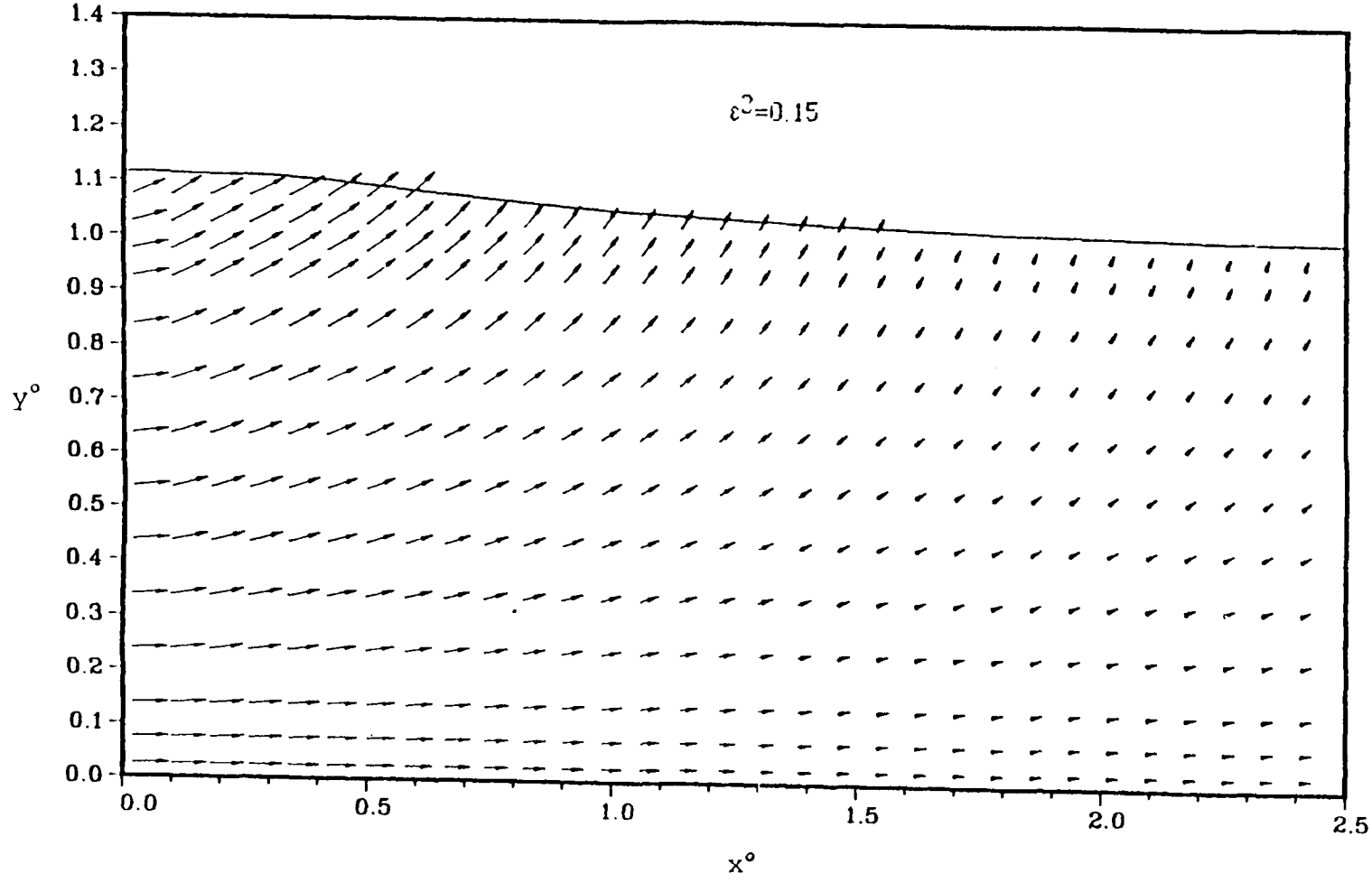

Figure 22. -- continued

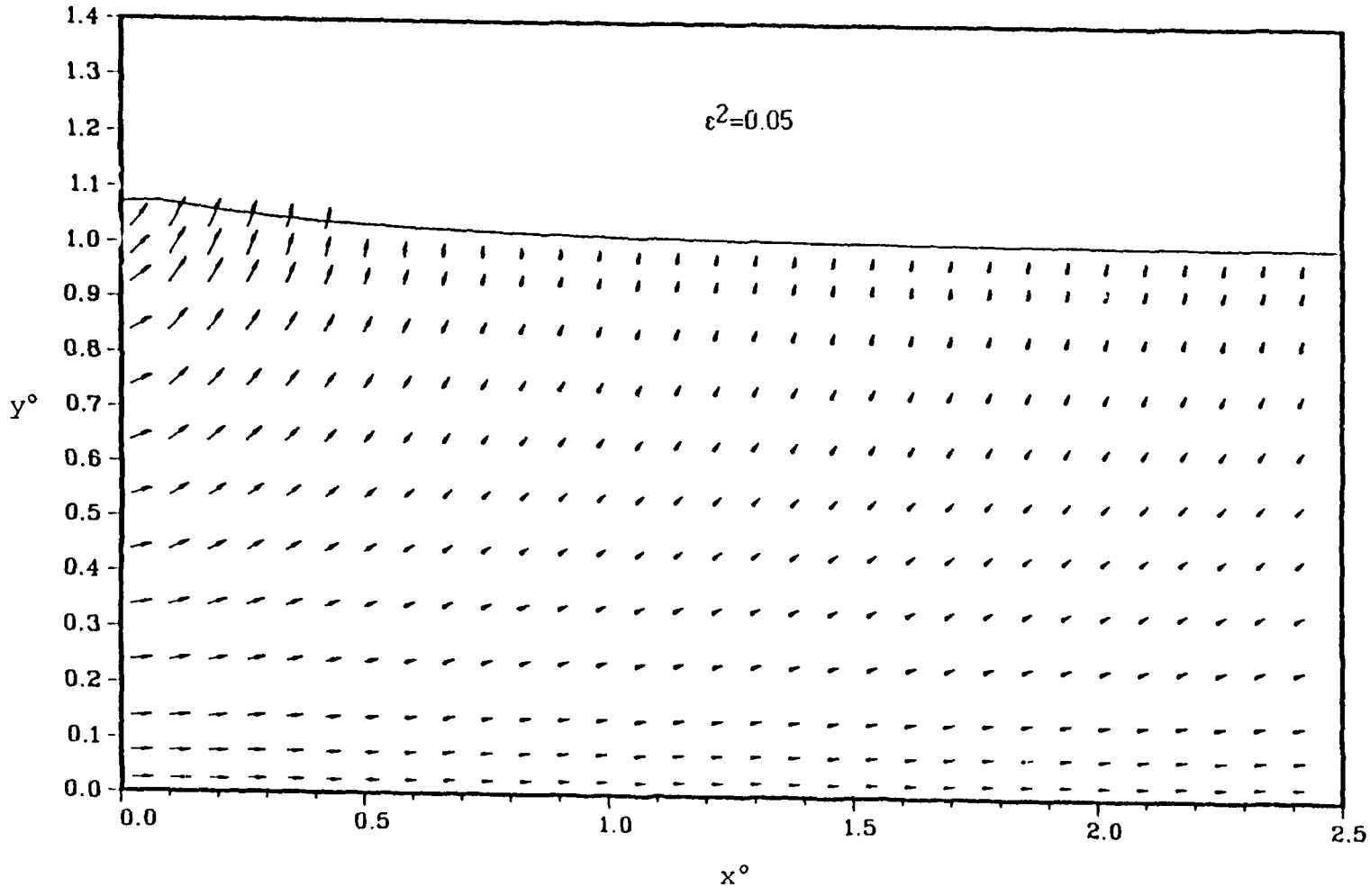

Figure 23. Time evolution of the velocity vector field ahead of the plate for a=0.78-0.69t (m/sec^2).

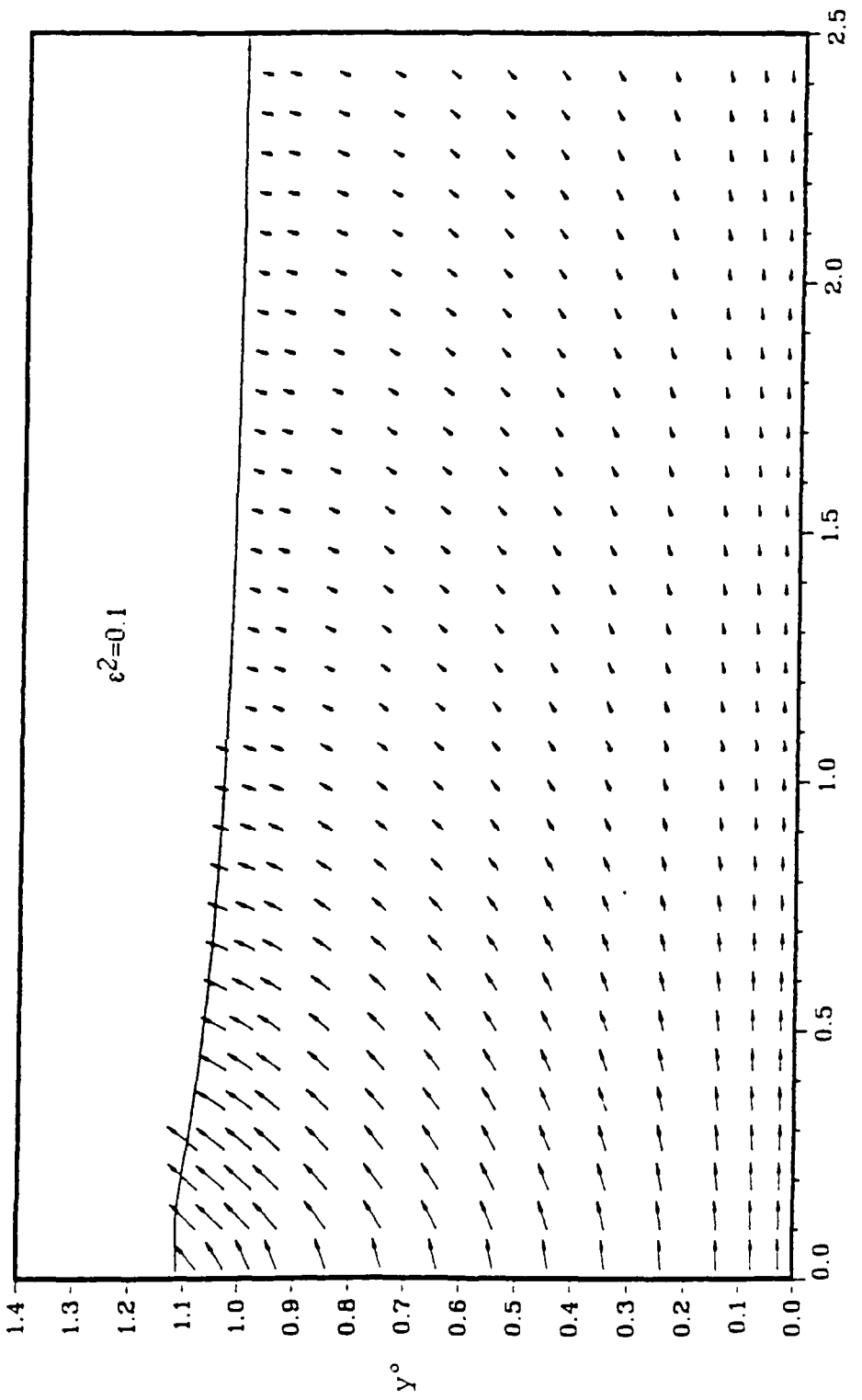

Figure 23. -- continued

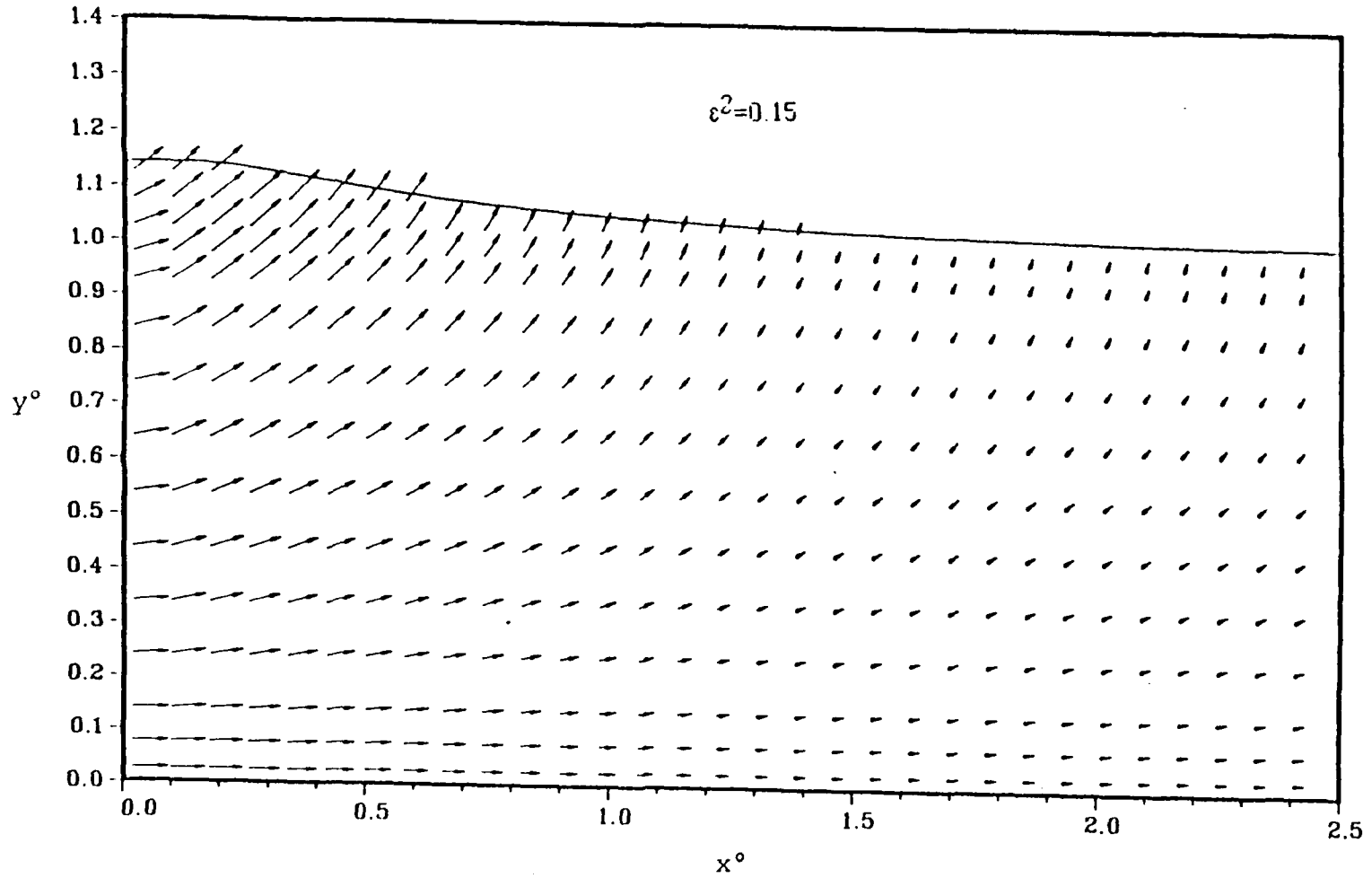

Figure 23. -- continued

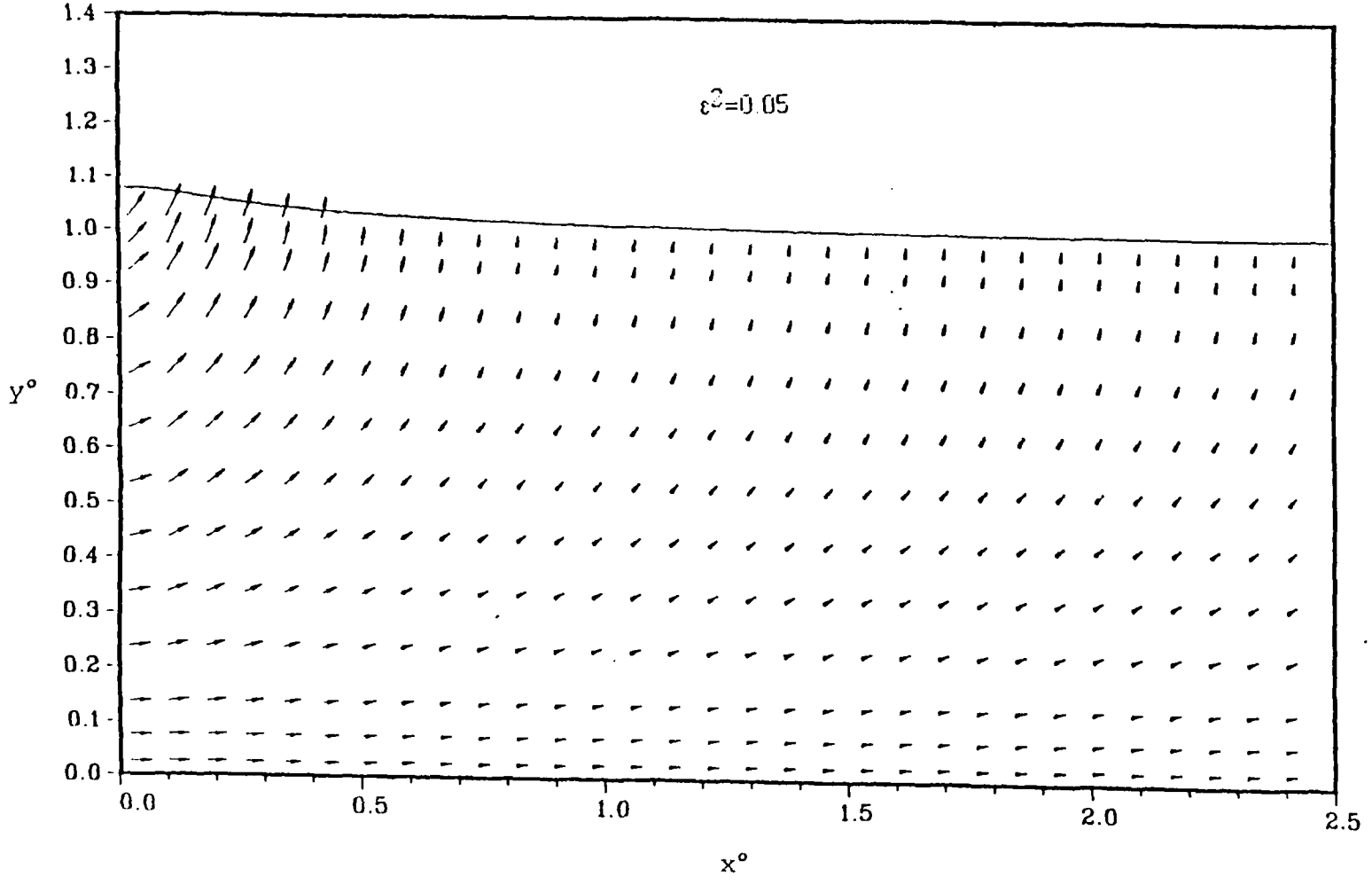

Figure 24. Time evolution of the velocity vector field ahead of the plate for a=1.04-0.96t (m/sec^2).

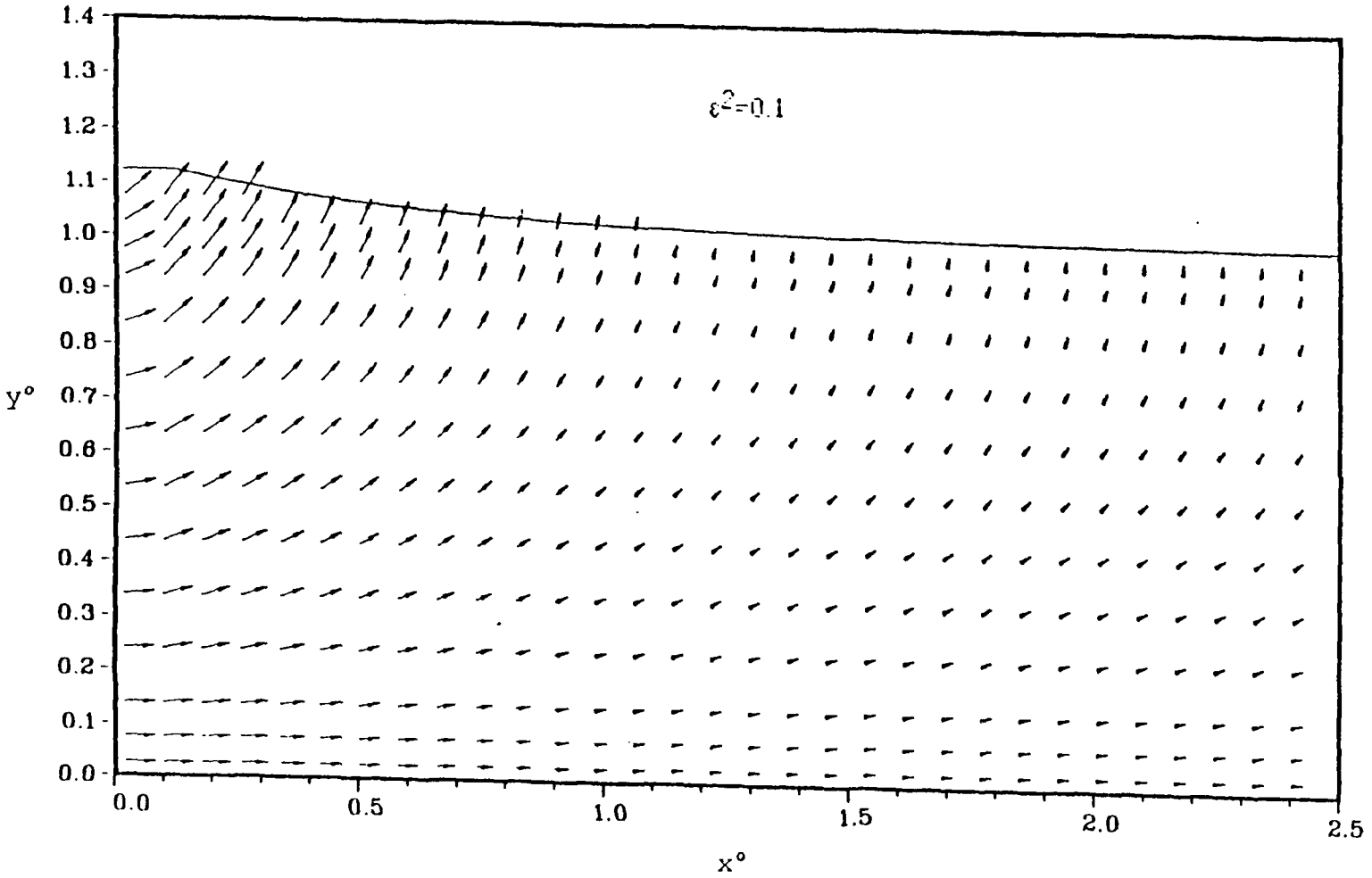

Figure 24. -- continued

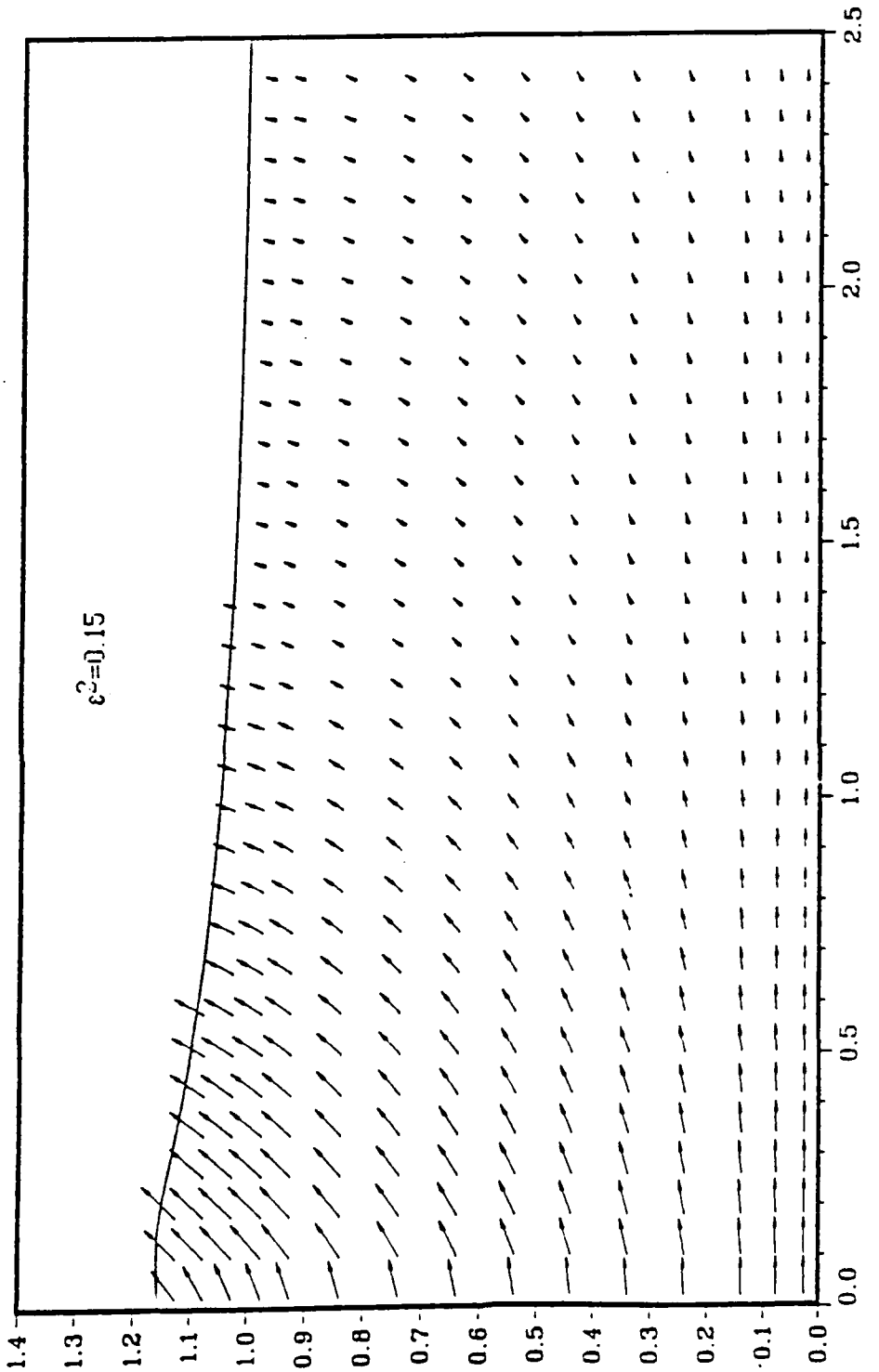

Figure 24. -- continued

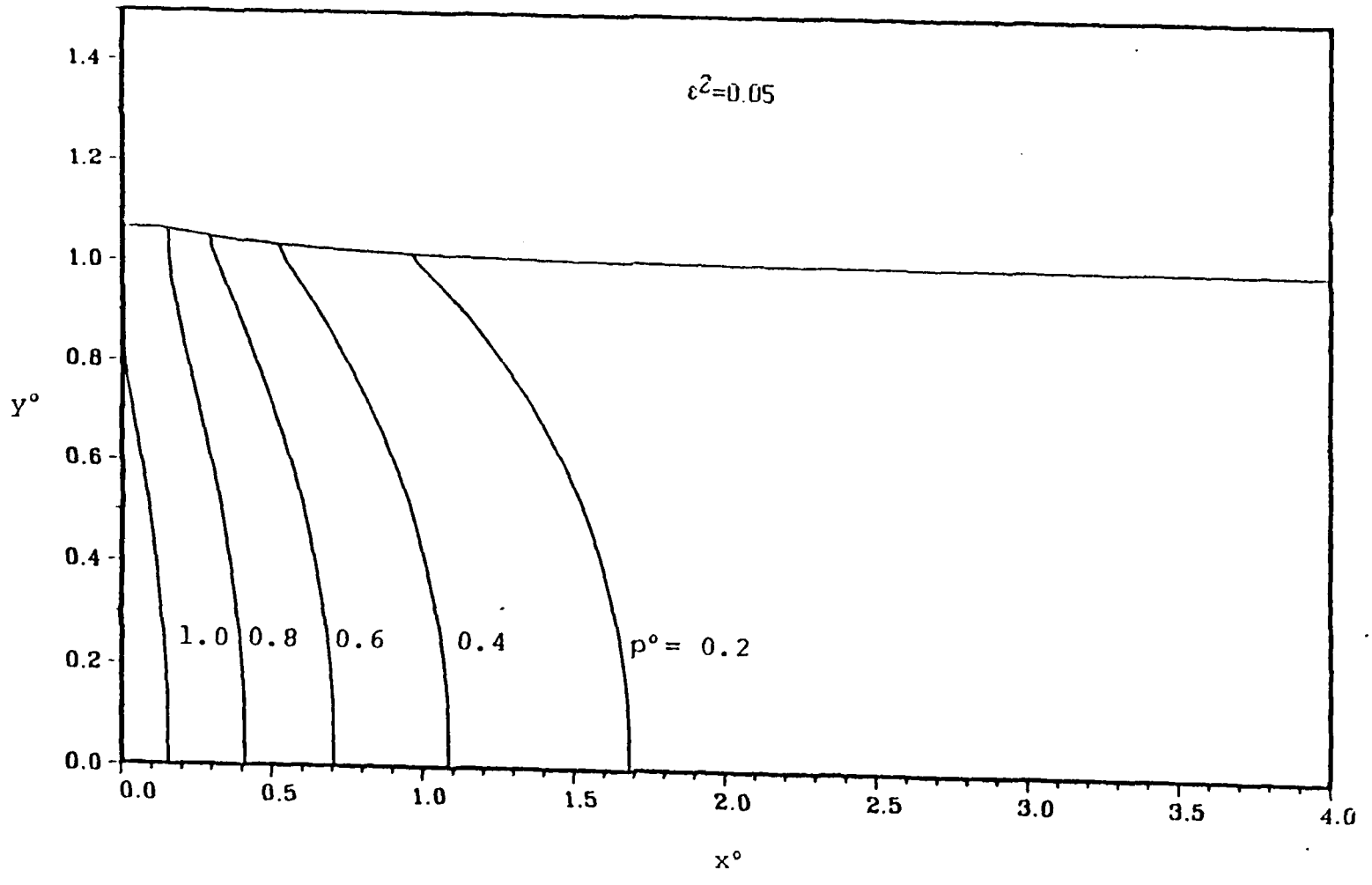

Figure 25. Time evolution of the pressure field ahead of the plate for a=0.55-0.55t (m/sec^2).

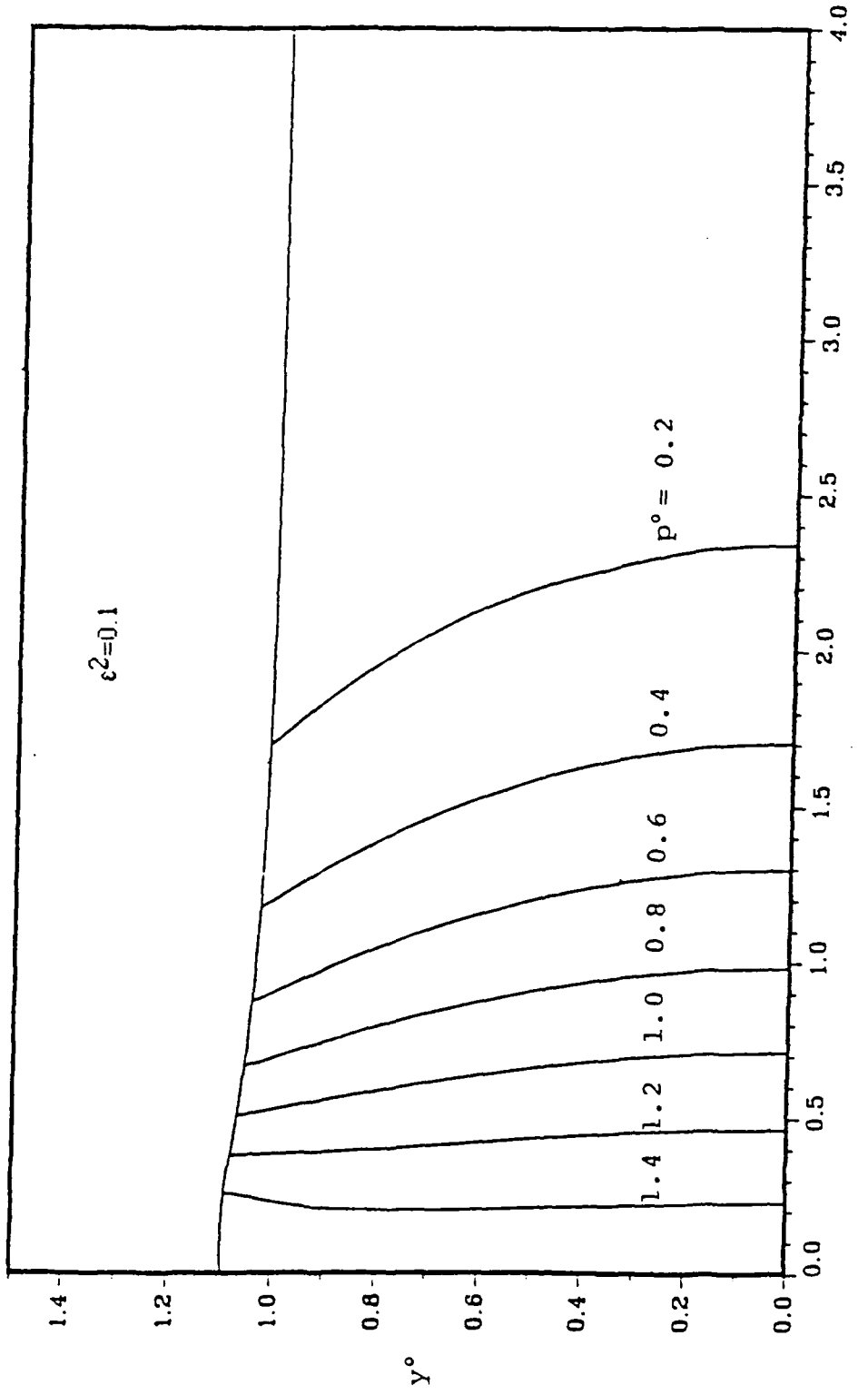

Figure 25. -- continued

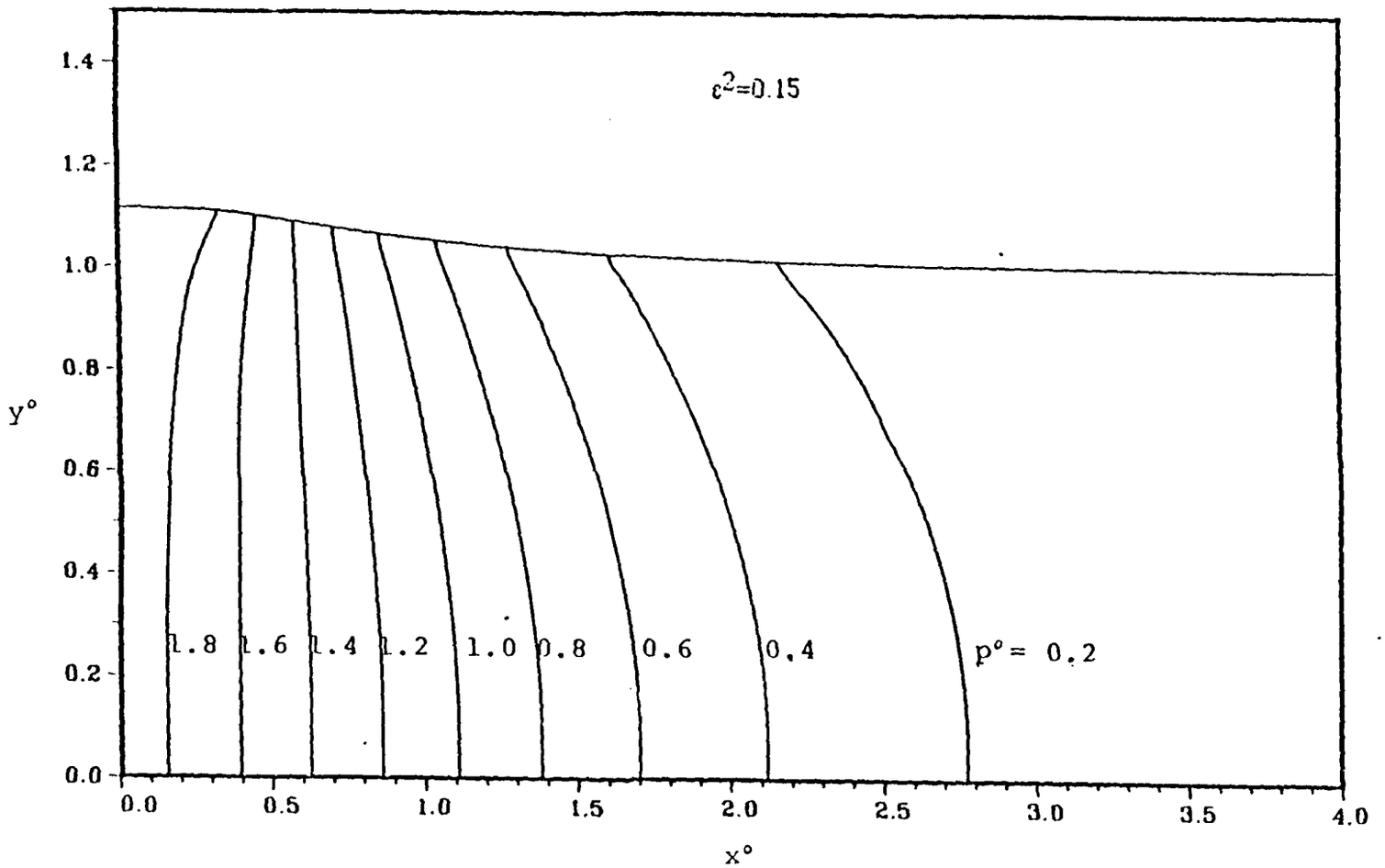

Figure 25. -- continued

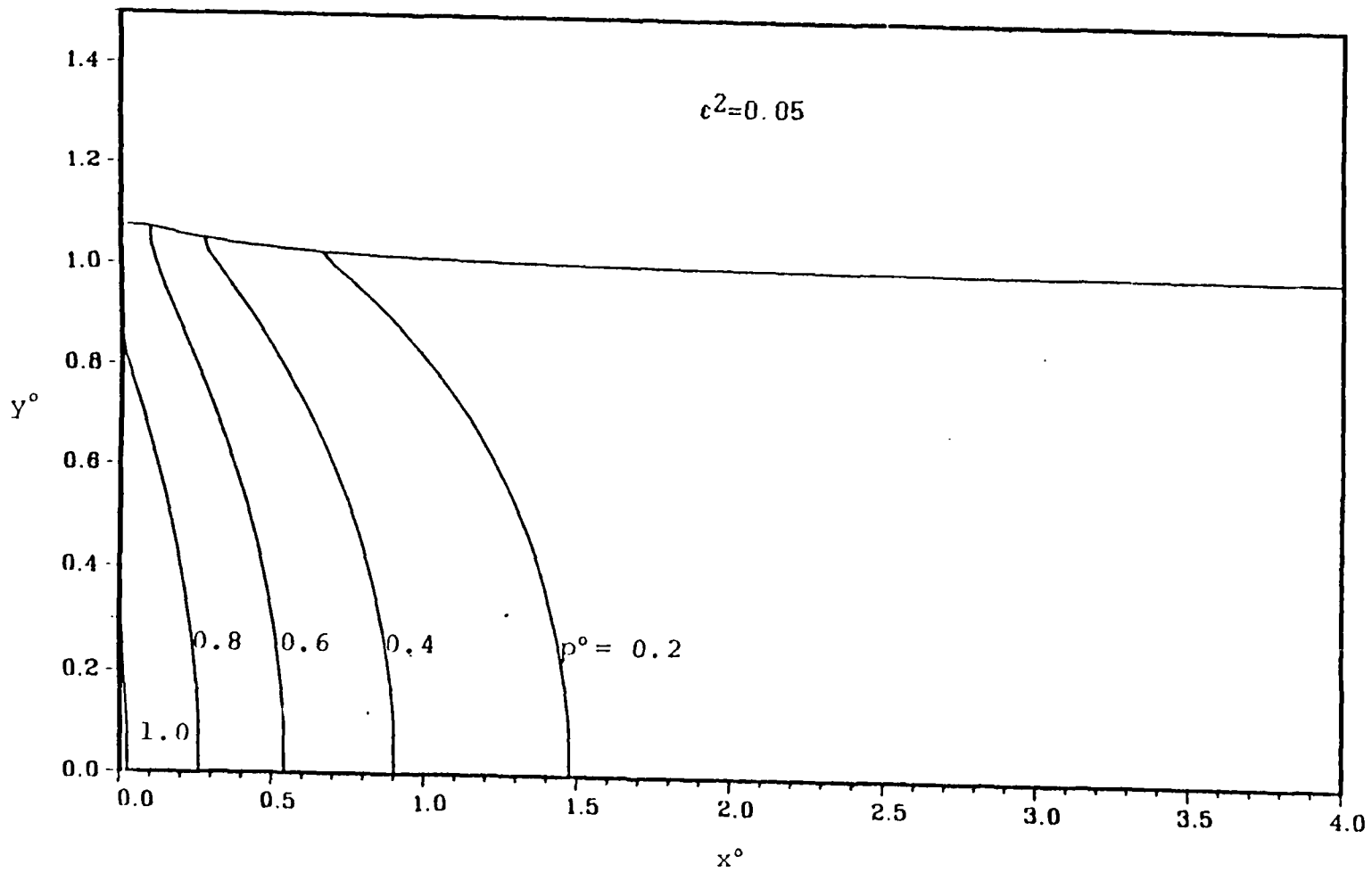

Figure 26. Time evolution of the pressure field ahead of the plate for a=0.86-0.88t (m/sec^2).

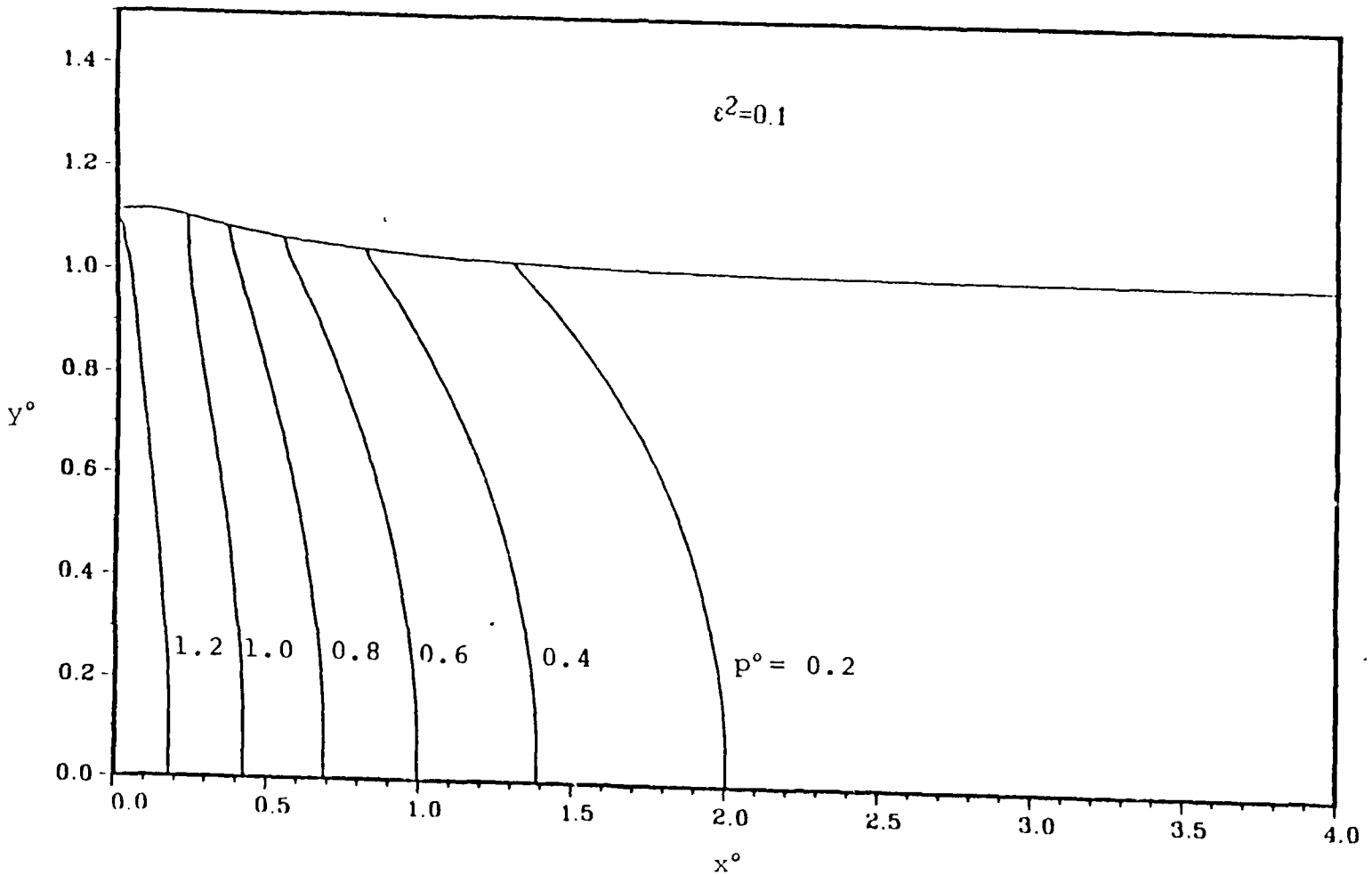

Figure 26. -- continued

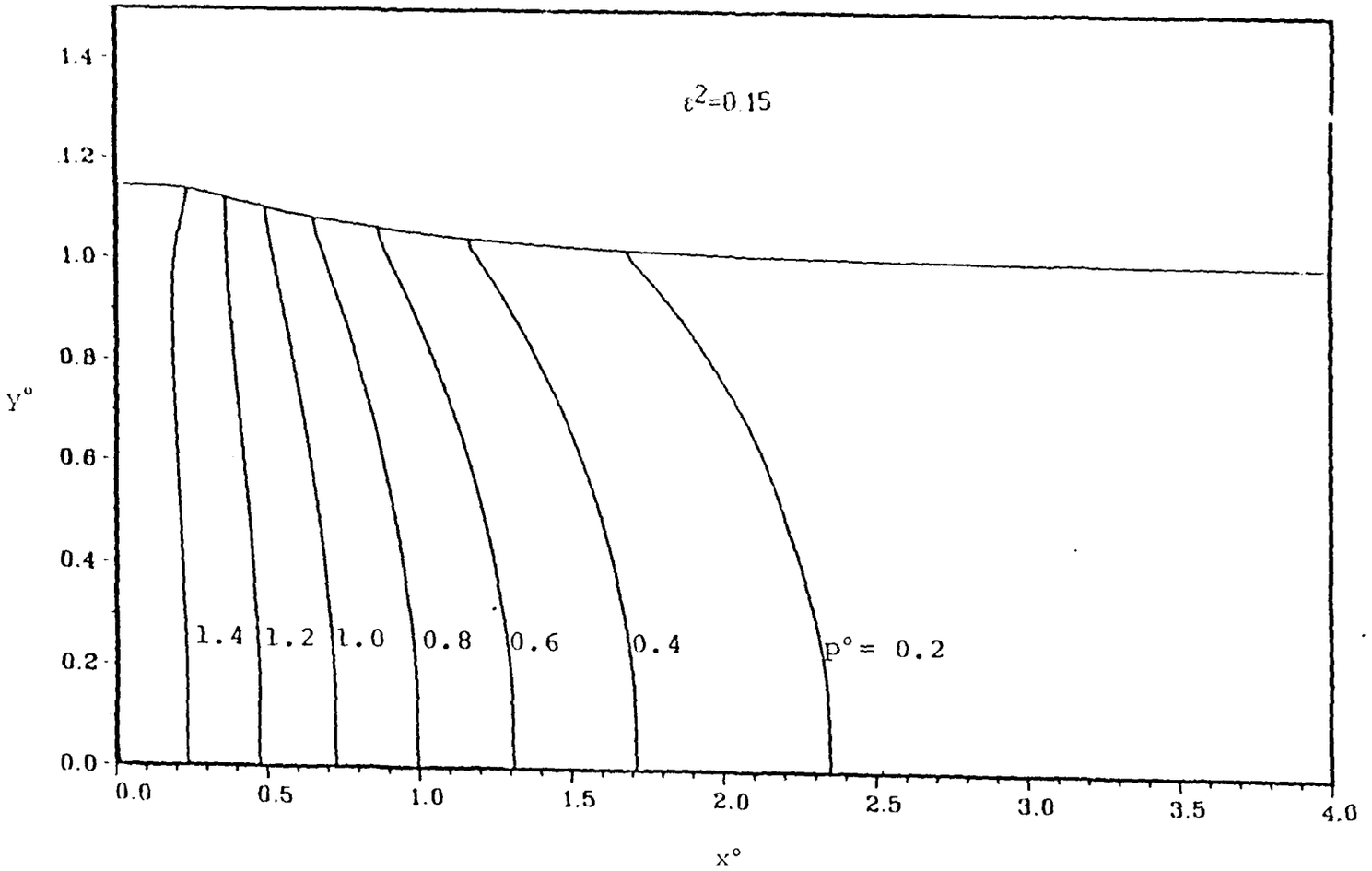

Figure 26. -- continued

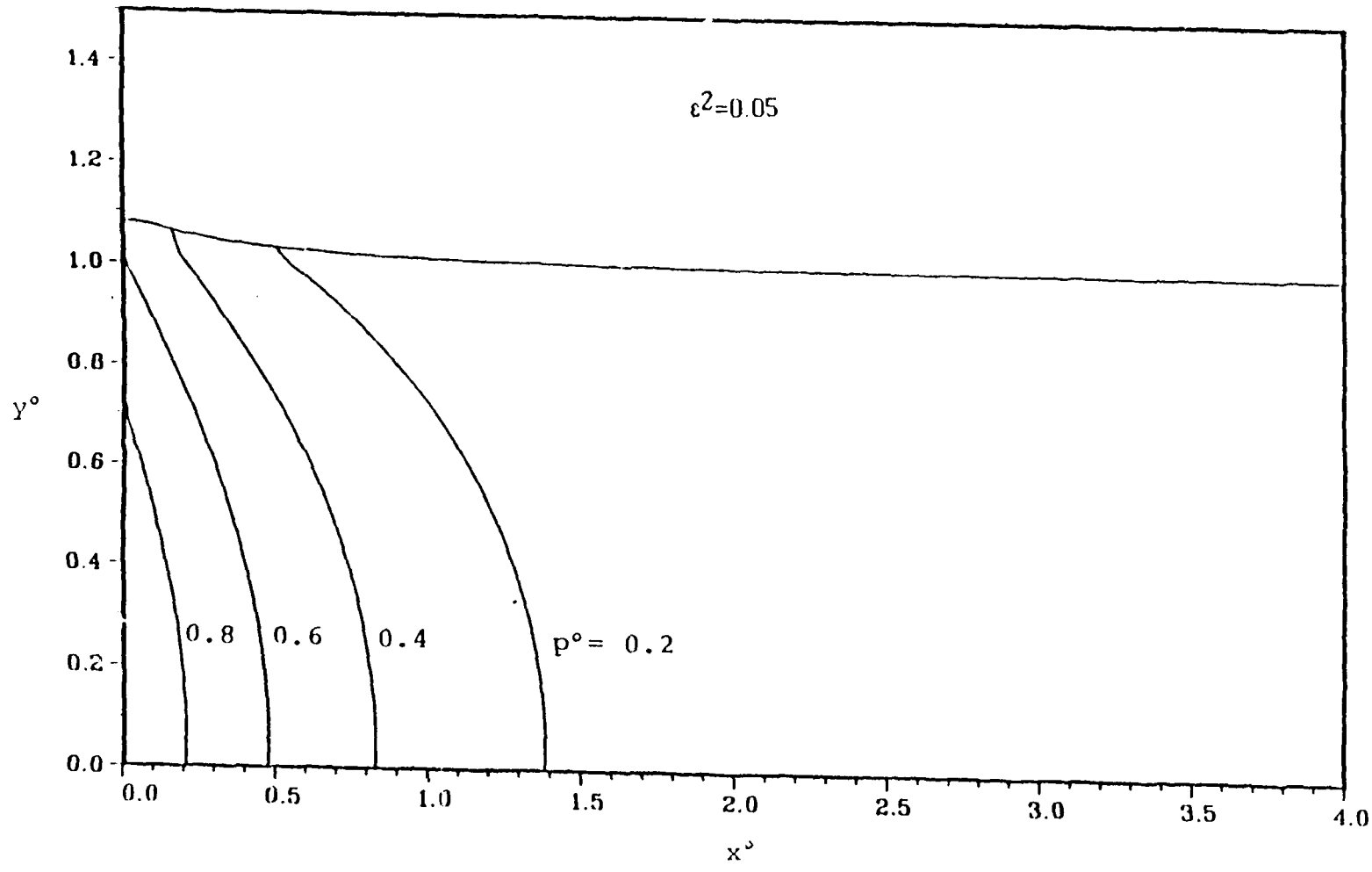

Figure 27. Time evolution of the pressure field ahead of the plate for a=1.12-1.11t (m/sec^2).

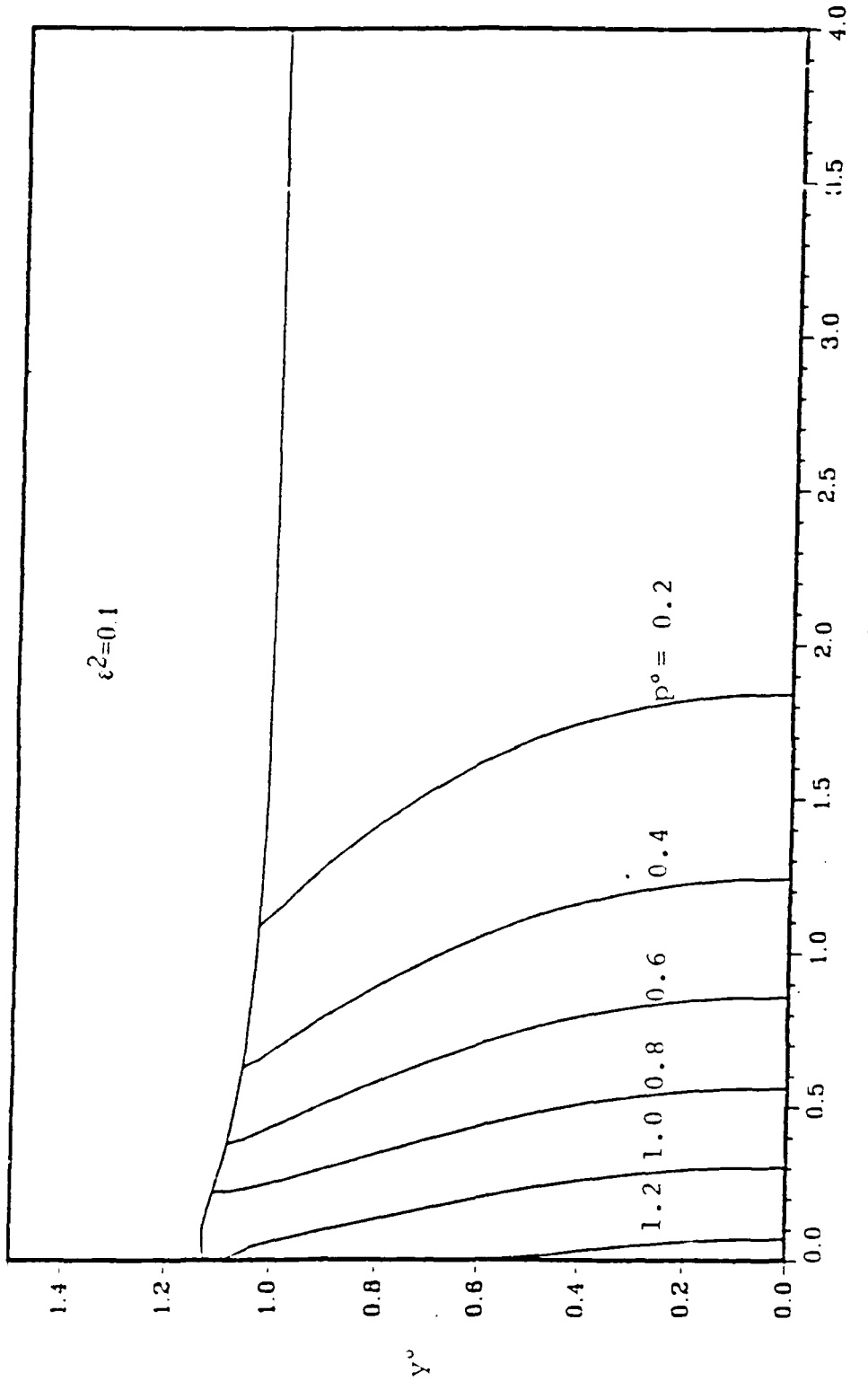

Figure 27. -- continued

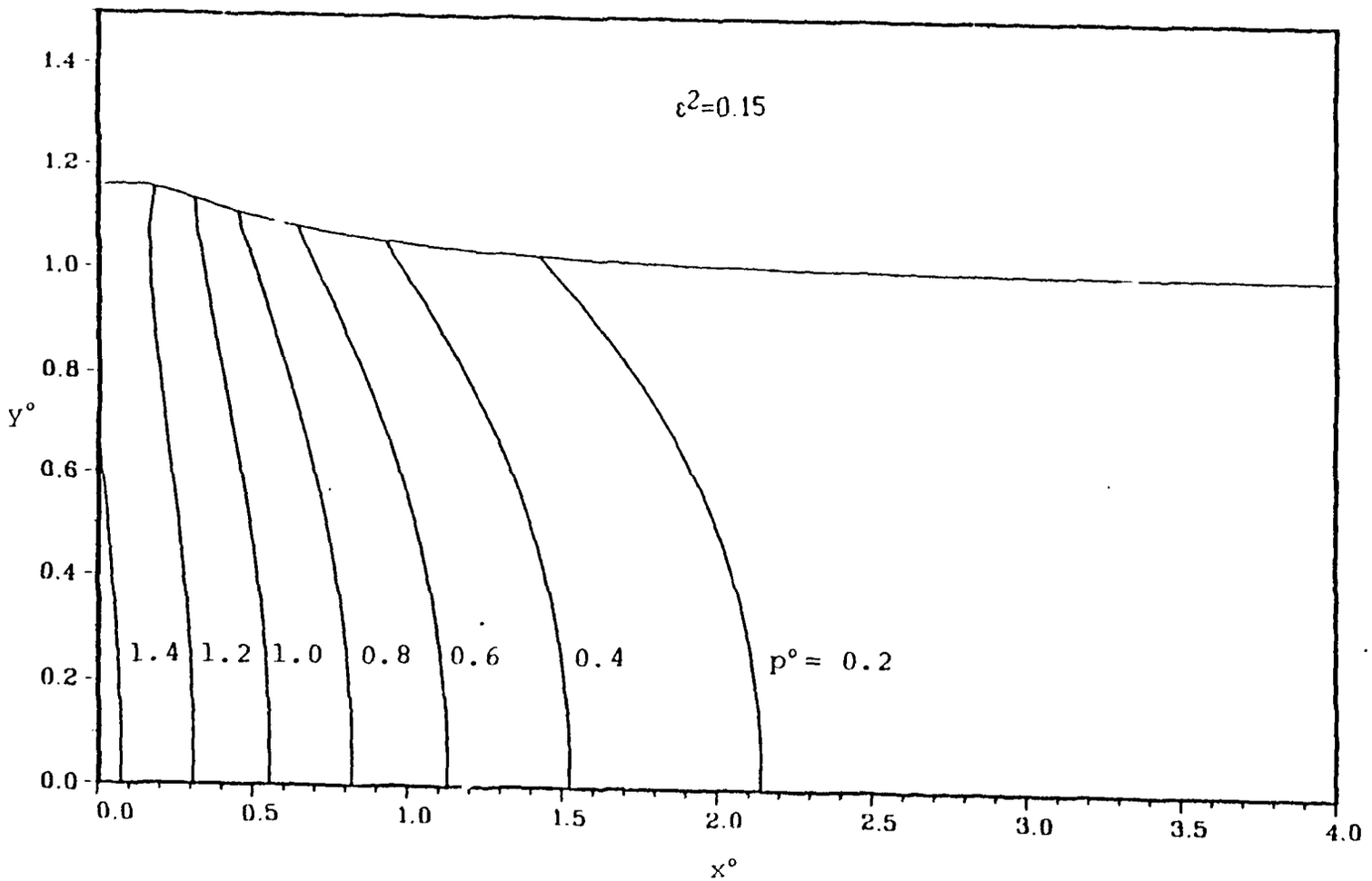

Figure 27. -- continued